Atmospheric
Chemistry
and Physics
Open Access

Seasonal and interannual variations in HCN amounts in the upper troposphere and lower stratosphere observed by MIPAS

N. Glatthor[1], M. Höpfner[1], G. P. Stiller[1], T. von Clarmann[1], B. Funke[2], S. Lossow[1], E. Eckert[1], U. Grabowski[1], S. Kellmann[1], A. Linden[1], K. A. Walker[3], and A. Wiegele[1]

[1]Karlsruher Institut für Technologie, Institut für Meteorologie und Klimaforschung, Karlsruhe, Germany
[2]Instituto de Astrofísica de Andalucía (CSIC), Granada, Spain
[3]Department of Physics, University of Toronto, Toronto, Canada

Correspondence to: N. Glatthor (norbert.glatthor@kit.edu)

Abstract. We present a HCN climatology of the years 2002–2012, derived from FTIR limb emission spectra measured with the Michelson Interferometer for Passive Atmospheric Sounding (MIPAS) on the ENVISAT satellite, with the main focus on biomass burning signatures in the upper troposphere and lower stratosphere. HCN is an almost unambiguous tracer of biomass burning with a tropospheric lifetime of 5–6 months and a stratospheric lifetime of about 2 years. The MIPAS climatology is in good agreement with the HCN distribution obtained by the spaceborne ACE-FTS experiment and with airborne in situ measurements performed during the INTEX-B campaign. The HCN amounts observed by MIPAS in the southern tropical and subtropical upper troposphere have an annual cycle peaking in October–November, i.e. 1–2 months after the maximum of southern hemispheric fire emissions. The probable reason for the time shift is the delayed onset of deep convection towards austral summer. Because of overlap of varying biomass burning emissions from South America and southern Africa with sporadically strong contributions from Indonesia, the size and strength of the southern hemispheric plume have considerable interannual variations, with monthly mean maxima at, for example, 14 km between 400 and more than 700 pptv. Within 1–2 months after appearance of the plume, a considerable portion of the enhanced HCN is transported southward to as far as Antarctic latitudes. The fundamental period of HCN variability in the northern upper troposphere is also an annual cycle with varying amplitude, which in the tropics peaks in May after and during the biomass burning seasons in northern tropical Africa and southern Asia, and in the subtropics peaks in July due to trapping of pollutants in the Asian monsoon anticyclone (AMA). However, caused by extensive biomass burning in Indonesia and by northward transport of part of the southern hemispheric plume, northern HCN maxima also occur around October/November in several years, which leads to semi-annual cycles. There is also a temporal shift between enhanced HCN in northern low and mid- to high latitudes, indicating northward transport of pollutants. Due to additional biomass burning at mid- and high latitudes, this meridional transport pattern is not as clear as in the Southern Hemisphere. Upper tropospheric HCN volume mixing ratios (VMRs) above the tropical oceans decrease to below 200 pptv, presumably caused by ocean uptake, especially during boreal winter and spring. The tropical stratospheric tape recorder signal with an apparently biennial period, which was detected in MLS and ACE-FTS data from mid-2004 to mid-2007, is corroborated by MIPAS HCN data. The tape recorder signal in the whole MIPAS data set exhibits periodicities of 2 and 4 years, which are generated by interannual variations in biomass burning. The positive anomalies of the years 2003, 2007 and 2011 are caused by succession of strongly enhanced HCN from southern hemispheric and Indonesian biomass burning in boreal autumn and of elevated HCN from northern tropical Africa and the AMA in subsequent spring and summer. The anomaly of 2005 seems to be due to springtime emissions from tropical Africa followed by release from the summertime AMA. The vertical transport time of the anomalies is 1 month or less between 14 and 17 km in the upper troposphere and 8–11 months between 17 and 25 km in the lower stratosphere.

1 Introduction

Hydrogen cyanide (HCN) is one of the most abundant atmospheric cyanides (Singh et al., 2003). The first spectroscopic detection of stratospheric HCN was reported by Coffey et al. (1981) and the first discovery of tropospheric HCN by Rinsland et al. (1982). Model calculations by Cicerone and Zellner (1983) resulted in rather uniform tropospheric HCN concentrations, which slowly declined with increasing altitude in the stratosphere. These authors identified reaction with OH as the main tropospheric sink and reaction with $O^1(D)$ as well as photodissociation as major stratospheric sinks, resulting in an atmospheric residence time of about 2.5 years. However, various measurements performed in later years (Mahieu et al., 1995, 1997; Rinsland et al., 1998, 1999, 2000, 2001a, 2001b, 2002) showed that tropospheric HCN exhibits strong seasonal and spatial variations, which is inconsistent with a tropospheric lifetime of several years. These observations led to the conclusion that biomass burning is a major source of atmospheric HCN and that there must be an additional sink of tropospheric HCN. Today, HCN is considered as an almost unambiguous tracer of biomass burning (Li et al., 2003; Singh et al., 2003; Yokelson et al., 2007; Lupu et al., 2009). HCN has been used as tracer of biomass burning by, for example, Glatthor et al. (2009) and Tereszchuk et al. (2013). The latter authors emphasised the advantage of HCN over CO, which has additional anthropogenic sources. In recent years ocean uptake has been assumed to be the additional, major sink of HCN. Inclusion of this process in model calculations constrained by aircraft observations leads to a tropospheric lifetime of 5–6 months (Li et al., 2000, 2003; Singh et al., 2003).

HCN and other pollutants released by extensive biomass burning can form persistent upper tropospheric plumes, e.g. the southern hemispheric biomass burning plume peaking in October and November, caused by combustion throughout the preceding dry season in austral spring in South America, central and southern Africa, and Australia. The spatial extension and composition of this plume has been investigated using various ground-based, airborne and spaceborne observations (Singh et al., 1996, 2000; Rinsland et al., 2001, 2005; von Clarmann et al., 2007; Glatthor et al., 2009). In El Niño years, characterised by dry periods in Indonesia, fire emissions from this region are a considerable additional contribution to tropical biomass burning in austral spring. Biomass burning in Indonesia is characterised by a high percentage of peat fires (van der Werf et al., 2010), which according to Akagi et al. (2011) release HCN amounts which are a factor of 10 higher than HCN emissions from savanna or tropical forest fires. Another region of enhanced upper tropospheric HCN is the Asian monsoon anticyclone (AMA), which is centred above southern Asia in June, July and August (Park et al., 2008, and references therein). Spaceborne observations of global HCN have been performed by the Fourier transform spectrometer of the Atmospheric Chemistry Experiment (ACE-FTS) on SCISAT (Bernath et al., 2005; Boone et al., 2005; Rinsland et al., 2005) and, generally restricted to the middle atmosphere, by the Microwave Limb Sounder (MLS) on the Aura satellite (Pumphrey et al., 2006). Climatologies of the HCN distribution derived from ACE-FTS measurements have been presented by Lupu et al. (2009), Randel et al. (2010) and Park et al. (2013).

Transport of tropospheric air masses into the stratosphere mainly occurs through the tropical tropopause (Holton et al., 1995). If a tropospheric source gas exhibits a temporal variation, this feature will propagate into the stratosphere and will be transported upward by the Brewer–Dobson circulation with a temporal lag, which increases with altitude. This phase shift is referred to as a tropical tape recorder and has been observed in water vapour, CO_2 and CO (Mote et al., 1996; Andrews et al., 1999; Schoeberl et al., 2006). First observations of a HCN tape recorder signal in MLS and ACE-FTS data were published by Pumphrey et al. (2008). These authors analysed the period July 2004 to June 2007 and found a period of 2 years, which is in contrast to the annual cycle of the tape recorder signals of water vapour, CO_2 and CO. They conclude that the reason for the 2-year cycle is not fully understood and suggest that it might be due to interannual variations in biomass burning in Indonesia. In subsequent publications these observations have been compared with model runs. Li et al. (2009) used ground-based HCN column amounts as well as MLS and ACE-FTS data to constrain the GEOS-Chem model, which resulted in annual and semi-annual variations in the upper troposphere but consecutive 2-year cycles of the HCN anomaly in the lower stratosphere. Their model runs indicated that the 2-year tape recorder cycle is caused by the extent of temporal overlap of biomass burning in Africa and other regions, particularly Indonesia, Australia and South America. On the other hand, interannual variations in the meteorology were shown to have little influence on the HCN amounts in the upper troposphere and lower stratosphere (UTLS) region. Pommrich et al. (2010) were able to reproduce the observed 2-year tape recorder signal with the Chemical Lagrangian Model of the Stratosphere (CLaMS) by use of temporally resolved biomass burning emissions from Indonesia. However, they expected an irregular cycle for a longer time series, because Indonesian biomass burning is strongly influenced by El Niño events. Park et al. (2013), who analysed a longer time series of tropical HCN from ACE-FTS, found tape recorder cycles of 1 and 2 years. Thus the question of whether there is a periodicity in the HCN tape recorder signal is still open, and the long time series of MIPAS (Michelson Interferometer for Passive Atmospheric Sounding) data is well suited for providing insight into this problem.

In the following we will briefly describe the MIPAS instrument and the HCN retrieval setup. In the discussion we will first discuss a seasonal climatology of the MIPAS HCN distribution and compare the MIPAS results with a HCN climatology established from ACE-FTS v2.2 data. Then, by

presenting time series of zonal averages of MIPAS HCN data of the upper troposphere and lower stratosphere, we will show that there are considerable interannual differences between the seasonal patterns. Through presentation of monthly global distributions we will illustrate the reasons for these differences. Finally, we will present the HCN tape recorder signal obtained from the whole MIPAS data set.

2 MIPAS measurements

2.1 Instrument description

The Michelson Interferometer for Passive Atmospheric Sounding (MIPAS) was operated onboard the European ENVIronmental SATellite (ENVISAT), which was launched into a Sun-synchronous polar orbit at about 800 km altitude on 1 March 2002. The satellite's Equator-crossing times are ∼10:00 and ∼22:00 LT. MIPAS is a limb-viewing Fourier transform infrared (FTIR) emission spectrometer covering the mid-infrared spectral region between 685 and 2410 cm^{-1} (4.1–14.6 μm), which enables simultaneous observation of numerous trace gases (European Space Agency (ESA), 2000; Fischer et al., 2008). MIPAS data were recorded from June 2002 until April 2012, when contact with ENVISAT was lost.
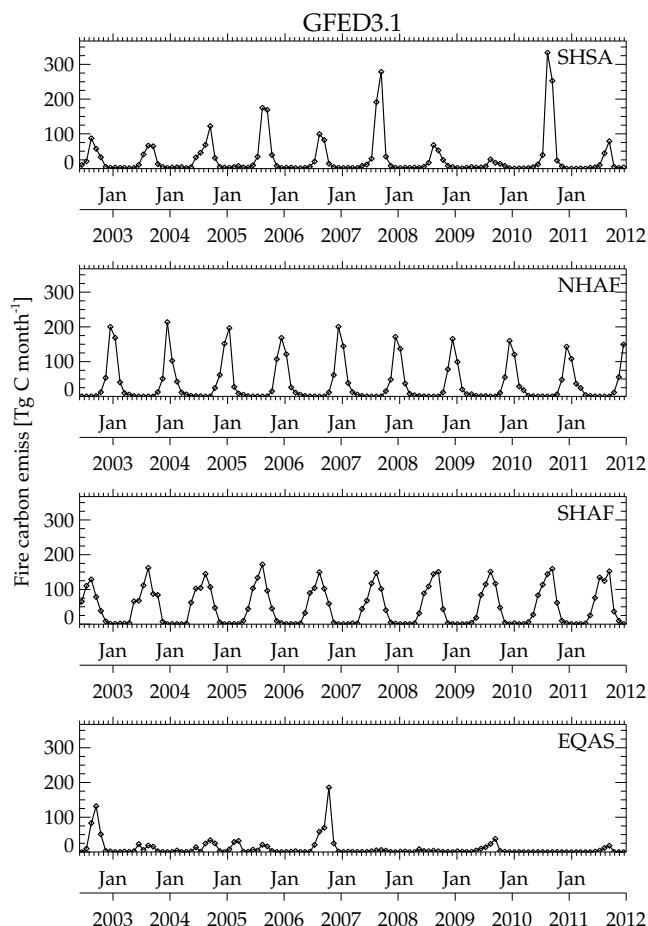
From June 2002 to April 2004 MIPAS was operated in its original high-resolution (HR) mode with a spectral resolution (sampling) of 0.025 cm^{-1} and a latitudinal sampling distance of ∼ 4.8° (530 km). After a data gap due to technical problems, MIPAS was run in the so-called reduced-resolution (RR) measurement mode with a spectral resolution of 0.0625 cm^{-1} and a latitudinal sampling distance of ∼ 3.6° (400 km) beginning in January 2005. We present data of the HR and of the RR "nominal" measurement modes, consisting of rearward limb scans covering the altitude region between 7 and 72 km within 17 and 27 altitude steps, respectively. The step width of the HR mode was 3 km up to 42 km and 5 to 8 km at higher altitudes. The step width of the RR "nominal" mode was 1.5 km up to 22 km, 2 km up to 32 km, 3 km up to 44 km and 4–4.5 km for the upper part of the scans. MIPAS was able to measure during day and night, and produced up to 1000 scans per day in original HR mode and up to 1400 scans per day in RR nominal mode. The level-1B radiance spectra used for retrieval are data version 5.02/5.06 (reprocessed data) provided by the ESA (Nett et al., 2002).

2.2 Retrieval method and error estimation

Retrievals were performed with the processor of the Institut für Meteorologie und Klimaforschung (IMK) and the Instituto de Astrofísica de Andalucía (IMK/IAA), using the Karlsruhe Optimized and Precise Radiative transfer Algorithm (KOPRA) (Stiller, 2000) for radiative transfer calculations and the Retrieval Control Program (RCP) of IMK/IAA for

inverse modelling. The inversion consists of derivation of vertical profiles of atmospheric state parameters from MIPAS level-1B spectra by means of constrained non-linear least-squares fitting in a global-fit approach (von Clarmann et al., 2003). Model spectra were calculated using the line list of the HIgh resolution TRANsmission (HITRAN) database (Rothman et al., 2013). Processing of MIPAS data at the IMK has been described in various papers, e.g. in von Clarmann et al. (2003) and Höpfner et al. (2004). Retrieval of HCN from MIPAS HR spectra has been described by Glatthor et al. (2009) and from RR spectra by Wiegele et al. (2012). The discussed data versions were V3O_HCN_2 and V5R_HCN_220, respectively.

Here we present the recently released data versions V5H_HCN_21 and V5R_HCN_222. The applied retrieval baseline differs from the previous ones in particular by the spectral windows used for analysis, which consist of 11 microwindows covering the spectral range 729.5–776.95 cm^{-1} for HR spectra and 729.5–776.9375 cm^{-1} for RR spectra. Compared to the previous baselines V3O_HCN_2 and V5R_HCN_220, an exactly intermediate regularisation strength was applied. Since the retrieval grid chosen has a finer altitude spacing than the height distance between the tangent altitudes, a constraint was necessary to attenuate instabilities. For this purpose, Tikhonov's first derivative operator was used (Steck, 2002, and references therein). This constraint does not try to shift the retrieved profile towards the a priori, but tends to maintain its vertical gradient only. To avoid any influence of the a priori information on the shape of the retrieved profiles, height-constant a priori profiles were chosen instead of climatological HCN profiles. Within the HCN retrieval, ozone was jointly fitted. Additional retrieval parameters fitted in each microwindow were atmospheric continuum profiles and corrections of calibration offsets. The radiative contribution of other interfering gases was modelled using their profiles as retrieved earlier in the processing sequence. When no prefitted profiles were available, the data of the MIPAS climatology (Remedios et al., 2007) were used. MIPAS single-scan measurements provide information on atmospheric HCN from the lower end of the profiles in the free troposphere up to about 45 km altitude. At 16 km altitude the total HCN retrieval error is about 6 and 8 % for high and background volume mixing ratios (VMRs), respectively. Towards 10 km the error increases to 15–30 % and towards 30 km it increases to 15 %. This error estimation contains measurement noise; uncertainties in temperature, instrumental pointing, and the VMRs of interfering species; and quasi-random instrumental errors. Spectroscopic uncertainties, which generally behave like systematic error contributions, have not been included. For the strongest lines used in MIPAS HCN retrieval, these uncertainties are between 5 and 10 % both for line intensity and for pressure broadening. More information on HCN error calculation can be found in Glatthor et al. (2009) and Wiegele et al. (2012). The verti-
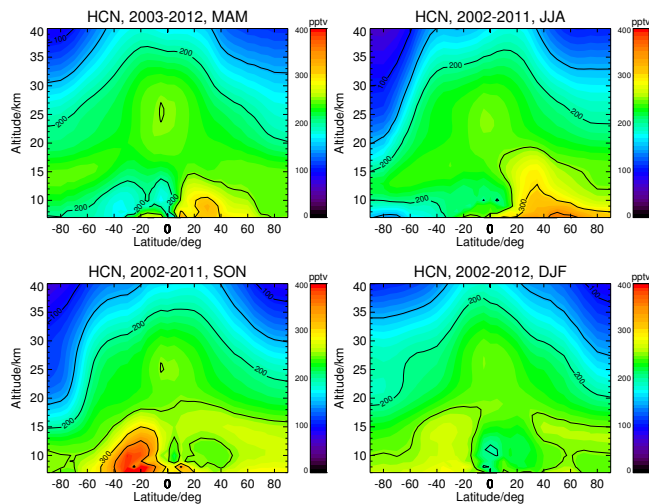
Figure 1. Monthly mean fire carbon emissions from the GFED3.1 database in southern hemispheric South America (SHSA), northern hemispheric Africa (NHAF), southern hemispheric Africa (SHAF) and equatorial Asia (EQAS) for the time period 2002 through 2011.
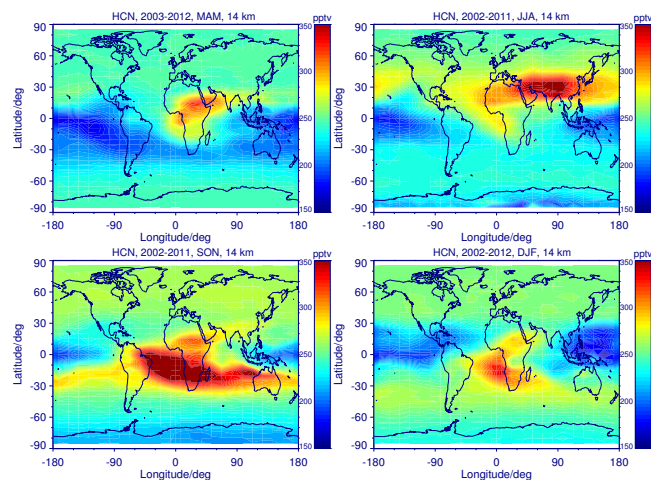

Figure 2. Climatological latitude–height cross sections of HCN volume mixing ratios measured by MIPAS during March to May (top left), June to August (top right), September to November (bottom left) and December to February (bottom right). The distributions are averaged over the time period 2002 to 2012.

cal resolution is 4–5 km in the altitude range 6 to 20 km and increases to 6 km at 25 km and to 8 km at 33 km.

3 Discussion of the HCN data set

3.1 GFED fire carbon emissions

For better interpretation of the MIPAS HCN data set we first present time series of biomass burning emissions of the Global Fire Emissions Database (GFED) (van der Werf et al., 2006, 2010). This database contains monthly emissions of various pollutants on a $0.5° \times 0.5°$ latitude–longitude grid for the time period 1997 to 2011. The emissions are based upon estimates of burned area and fire detections of the MODerate resolution Imaging Spectroradiometer (MODIS) sensor. Figure 1 shows GFEDv3 fire carbon emissions [Tg C month^{-1}] during the period of MIPAS operation from regions with most intensive biomass burning. These regions are southern hemispheric South America (SHSA), northern

hemispheric Africa (NHAF), southern hemispheric Africa (SHAF) and equatorial Asia (EQAS). A map of these regions and fire carbon emissions from additional regions can be found in van der Werf et al. (2006, 2010). According to the GFED time series, carbon emissions from South America and Africa exhibit regular annual cycles, whereas high emissions from equatorial Asia occurred in 2002 and 2006 only. While the amplitude of African carbon emissions fluctuates only moderately over the displayed period, South American emissions exhibit strong interannual variations, with especially strong events in 2007 and 2010. South American and southern hemispheric African fire emissions peak during August/September, those of northern hemispheric Africa during December/January and those of equatorial Asia (Indonesia) during September/October.

3.2 Seasonal climatology

Figure 2 shows latitude–height cross sections of MIPAS HCN VMRs measured in boreal spring, summer, autumn and winter, averaged over the whole measurement period 2002–2012. Averaging was performed for $7.5° \times 1$ km latitude–altitude bins at the poles and $5° \times 1$ km latitude–altitude bins elsewhere. Above 10 km altitude the averages are generally based on 10 000–15 000 values. Due to cloud contamination and the upward shift of the MIPAS RR-mode scans towards low latitudes, increasingly fewer data points could be binned at 10 km and below, e.g. only a few dozen or even less than 10 values at 7 km altitude in the tropics. The standard deviation of the mean values is less than 1 pptv in the stratosphere, less than 2 pptv in the upper troposphere and increases up to 10–20 pptv below 10 km altitude in the tropics. During all sea-

Figure 3. Climatological global HCN distributions measured by MIPAS during March to May (top left), June to August (top right), September to November (bottom left) and December to February (bottom right) at 14 km altitude. The distributions are averaged over the time period 2002 to 2012. Here and in subsequent contour plots values exceeding the displayed VMR range are also displayed in dark red.

sons the background HCN amounts in the undisturbed upper troposphere and lower and middle stratosphere are between 200 and 250 pptv (green areas).

From March to May (Fig. 2, top left) enhanced tropospheric values of up to 300 pptv were observed at northern tropical to mid-latitudes, caused by biomass burning in northern tropical Africa (see Figs. 1, 3), southeastern Asia (Hsu et al., 2003; van der Werf et al., 2010) and presumably Russia (Stohl et al., 2007; Warneke et al., 2010; see also fire emissions at NASA's Earth Observatory website, http://earthobservatory.nasa.gov/). Near 20° N the HCN plume extends up to 14 km altitude. Between southern tropics and mid-latitudes, very low tropospheric HCN amounts of less than 200 pptv were measured. This minimum is probably caused by ocean uptake (cf. Li et al., 2000, 2003; Singh et al., 2003) during a long period without southern hemispheric biomass burning. Because of its long middle atmospheric lifetime of 2.5 years (Cicerone and Zellner, 1983), stratospheric HCN is able to map seasonal cycles. The stratospheric HCN distribution is characterised by upwelling above the tropics and a general decrease with altitude and towards high latitudes.
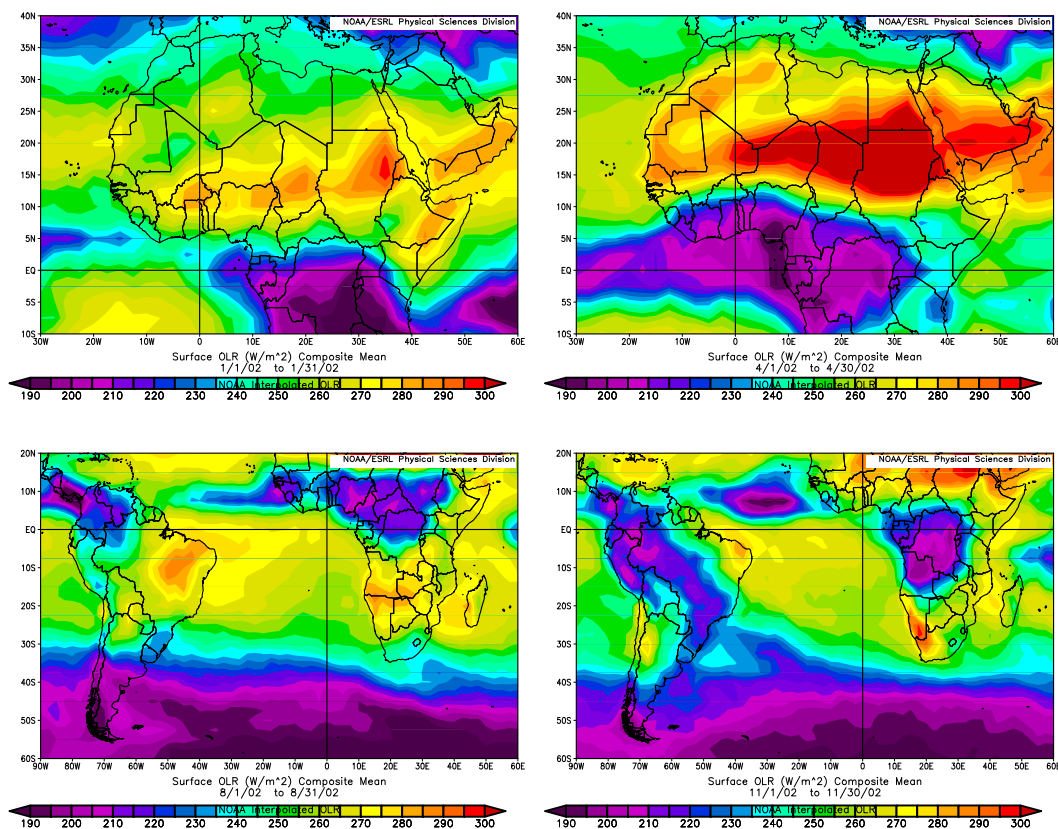
The latitude–height cross section of boreal summer (Fig. 2, top right) exhibits enhanced tropospheric HCN amounts at northern mid- to polar latitudes, reflecting intensified northern hemispheric biomass burning (cf. Tereszchuk et al., 2013). Due to trapping of pollutants in the Asian monsoon anticyclone (AMA) (cf. Fig. 3), the vertical extent of the HCN plume in the northern subtropics has considerably increased. At 30° N it reaches up to ~18 km altitude. Enhanced HCN amounts inside the AMA, extending as high

as into the lower stratosphere, have also been observed by ACE-FTS (Randel et al., 2010). These authors emphasise the importance of the AMA for transport of elevated HCN amounts into the stratosphere. Compared to boreal spring, tropospheric HCN amounts in the tropics have somewhat increased, but there are very low HCN amounts at mid- to high southern latitudes. Due to subsidence of mesospheric air masses in the Antarctic vortex, low stratospheric HCN amounts were observed at high southern latitudes during this season.

The cross section of boreal autumn (Fig. 2, bottom left) exhibits the highest HCN amounts of up to 400 pptv in a large area covering the southern tropics, subtropics and mid-latitudes. This strong signature is caused by intensive southern hemispheric biomass burning in boreal autumn (cf. Fig. 1; Edwards et al., 2006; Glatthor et al., 2009). The plume of enhanced HCN amounts extends up to about 17 km altitude in the subtropics. Elevated HCN values in the northern tropical UTLS are remnants of the AMA, strengthened by fresh pollution from the Southern Hemisphere (cf. Fig. 3). Further, the increase of lower stratospheric HCN amounts at northern high latitudes indicates northward transport of pollutants from inside the former AMA. Transport from the low-latitude upper troposphere into the extratropical lower stratosphere has, for example, been shown by Randel and Jensen (2013). The low-latitude tropospheric HCN minimum is now situated in the northern tropics to mid-latitudes. However it is somewhat weaker than its southern hemispheric counterpart in boreal spring. At high southern latitudes, stratospheric HCN amounts are comparably low compared to the previous season, reflecting the persistence of the Antarctic vortex, but the tropospheric minimum has been filled up again.

The northern tropospheric HCN amounts are lowest in boreal winter (Fig. 2, bottom right), reflecting interruption of biomass burning or ineffective transport of the fire emissions to levels within the vertical coverage of MIPAS. Due to decreased emissions and ocean uptake the tropospheric minimum at tropical latitudes has become stronger again. Mid- and upper stratospheric HCN is now lowest at high northern latitudes, which is caused by subsidence in the Arctic vortex. Compared to the previous season, the southern hemispheric biomass burning plume is diluted and has expanded southward, at altitudes above 10 km up to ~55° S and in the troposphere up to high southern latitudes (cf. Sect. 3.4).

To give an overview of the horizontal distribution of climatological HCN with the focus on the tropical and subtropical upper troposphere, Fig. 3 shows the seasonal variation at 14 km altitude. A similar presentation of HCN measured by ACE-FTS can be found in Randel et al. (2010, Fig. S1 in the Supplement). In boreal spring (top left), enhanced HCN, resulting from biomass burning in western and northern tropical Africa, forms a plume covering the whole of tropical Africa and parts of the surrounding oceans. However, the peak of fire emissions in northern tropical Africa is earlier around December/January (Fig. 1), when the north-
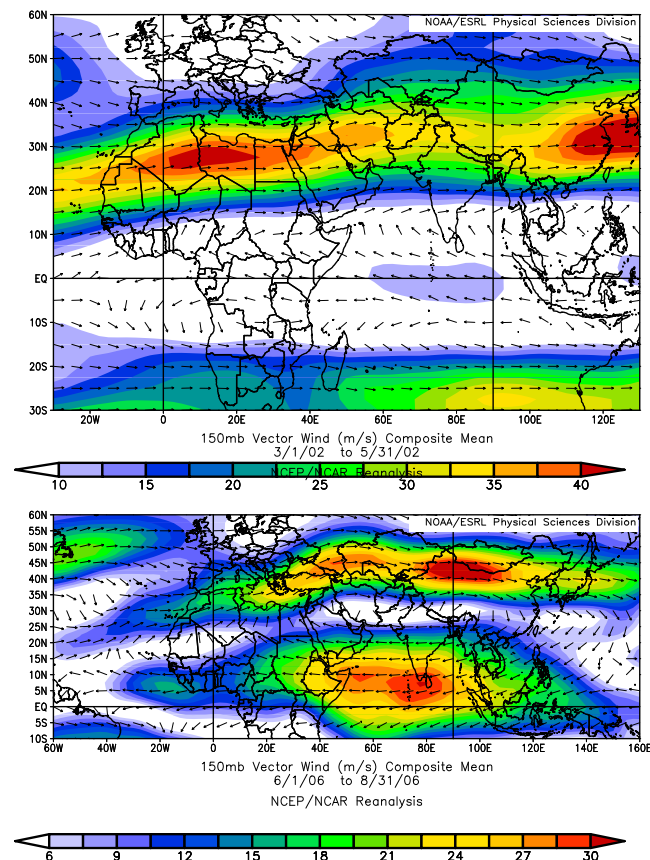
Figure 4. Outgoing longwave radiation (OLR) from northern Africa in January (top left) and April 2002 (top right), as well as from South America and Africa in August (bottom left) and November 2002 (bottom right). OLR values $\leq 220\,\mathrm{W\,m^{-2}}$ indicate deep convection. The plots were provided by the NOAA/ESRL Physical Sciences Division, Boulder, Colorado, from their website at http://www.esrl.noaa.gov/psd/.

ern African plume (Fig. 3, bottom right) is still weaker. A possible reason for the delay is more effective lifting in boreal spring, when deep convection above Africa has moved northward above the Equator. In order to illustrate the northward shift of deep convection we show the outgoing longwave radiation (OLR) of January and April 2002 from the NCEP/NCAR reanalysis (Kalnay et al., 1996; Liebmann and Smith, 1996), provided by the NOAA/ESRL Physical Sciences Division (Fig. 4, top). In January, low OLR values ($\leq 220\,\mathrm{W\,m^{-2}}$) indicating high cloud-top altitudes are nearly completely restricted to the regions south of the Equator, but in April the area of deep convection has moved northward to 10° N and covers the northern African biomass burning region. The northern part of the African plume is transported over southern Asia to as far as the eastern Pacific by the northern subtropical jet. To a lesser extent, the southern part of the plume is also transported eastward over Madagascar to northern Australia. Both pathways are confirmed by the springtime NOAA/ESRL wind field at the 150 hPa level (Fig. 5, top). The wind field shows the entrainment of air masses from northern tropical Africa by the northern subtropical jet and of air masses over the Gulf of Guinea by the southern subtropical jet. The low HCN amounts observed

above the southern tropical and subtropical Pacific, Indonesia, Australia, and the southern subtropical Indian and Atlantic Ocean suggest ocean uptake.

The main feature during boreal summer (Fig. 3, top right) is considerably enhanced HCN extending from the northwest African coast over southern Asia to the western Pacific, i.e. over the central AMA region and its western and eastern outskirts. Figure 5 (bottom) shows the NOAA/ESRL wind field of summer 2006 at the 150 hPa level as an example of the extension of the AMA. The anticyclone covers northern hemispheric low to mid-latitudes mainly between northeastern Africa and the Chinese coast, but its outer boundary extends westward over the mid-Atlantic and eastward over the western Pacific. Due to dispersal of enhanced HCN presumably from west and central African biomass burning into southern low latitudes, the HCN amounts above the southern tropical and subtropical oceans have increased as compared to boreal spring.

Caused by southern hemispheric biomass burning, the most extensive plume was observed in boreal autumn in the southern tropics and subtropics (Fig. 3, bottom left). It extends from South America over southern Africa to Australia and, driven by the southern subtropical jet, further around

Figure 5. Wind vectors at the 150 hPa level over Africa, Europe and Asia for the periods March to May 2002 (top) and June to August 2006 (bottom). Underlying colours indicate wind speed in $m\,s^{-1}$. The plots were provided by the NOAA/ESRL Physical Sciences Division, Boulder, Colorado, from their website at http://www.esrl.noaa.gov/psd/.
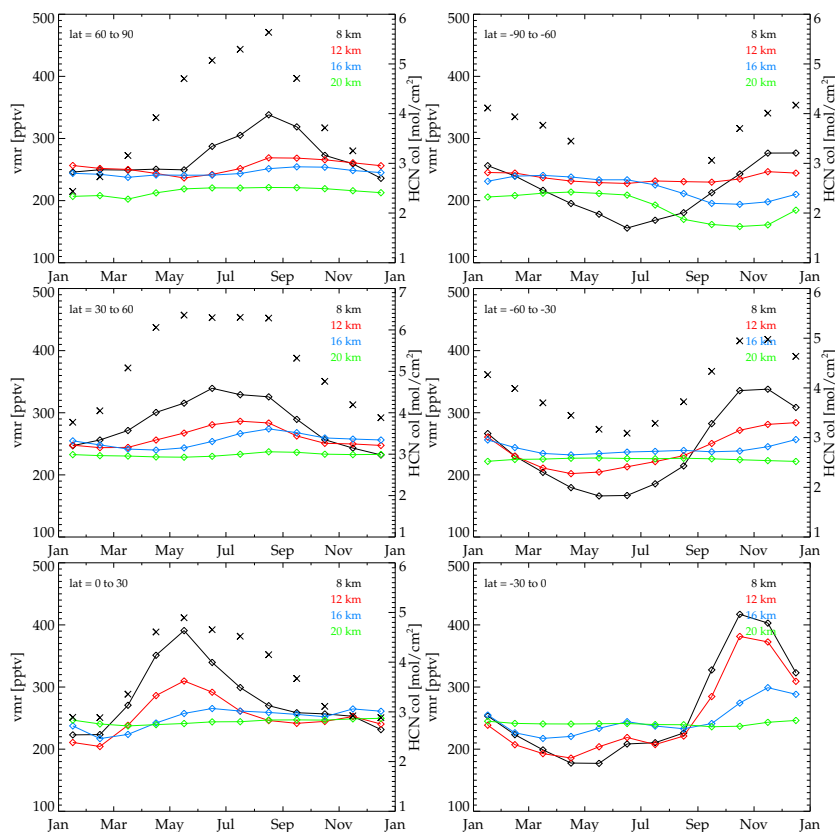
the globe above the southern tropical Pacific. Like in boreal spring, a smaller part of the polluted air masses is transported northeastward from Africa over southern Asia to China. There is only a weak signature of biomass burning above Indonesia and tropical Australia in this climatology, because during most of the years fire emissions from this region were rather low (see Fig. 1). The slightly increased lower stratospheric HCN amounts at northern mid- and high latitudes obviously originate from the former AMA (cf Fig. 2, bottom left). Due to strong biomass burning, the minimum above the tropical oceans is least distinct in this season.

The distribution of boreal winter (Fig. 3, bottom right) shows the remnants of the southern hemispheric plume, which in the meantime has been considerably diluted. The highest HCN amounts are located above the southern tropical and subtropical Atlantic as well as southern and northeastern Africa. Moderately enhanced HCN amounts now cover southern mid-latitudes up to 50° S, showing southward expansion of the plume (cf. Sect. 3.4). Similar to the North-

ern Hemisphere in boreal autumn, increased HCN amounts at high southern latitudes indicate transport from the lower latitude upper troposphere into the extratropical lower stratosphere. Due to less biomass burning, the minimum above the tropical oceans has increased in comparison to the preceding season.

In Fig. 6 we present time series of monthly climatological HCN observed by MIPAS at 8, 12, 16 and 20 km altitude in six different latitude bands and HCN column amounts retrieved from ground-based FTIR measurements at stations of the Network for the Detection of Atmospheric Composition Change (NDACC) in the respective latitude bands (http://www.ndsc.ncep.noaa.gov/). These stations are Kiruna (Sweden, 67.8° N), Toronto (Canada, 43.6° N), Izaña (Tenerife, 28.3° N), Lauder (New Zealand, 45.0° S) and Arrival Heights (Antarctica, 77.8° S). For the latitude band 0–30° S, HCN column amounts from NDACC stations are not available. Since the major contribution to these column amounts results from the troposphere (Rinsland et al., 1999, 2000), the seasonal changes in these amounts can be compared to the variation in tropospheric HCN observed by MIPAS.

The largest seasonal variations occur at the altitude of 8 km, which is tropospheric at low and mid-latitudes and in the tropopause region at high latitudes. As already mentioned above, the tropospheric maxima observed at northern mid-latitudes in June and at northern high latitudes in August are caused by agricultural fires, e.g. in eastern Europe in spring (Stohl et al., 2007); by boreal biomass burning (Tereszchuk et al., 2013); and partly by northward transport of pollutants released at lower latitudes. The enhanced values of nearly 400 pptv in the northern tropics and subtropics in May result from emissions from northern Africa (cf. Fig. 3) and from springtime biomass burning in southeastern Asia. The strong maxima in the latitude bands 0–30 and 30–60° S during October and November are caused by biomass burning in South America, southern Africa and Indonesia. Their temporal delay of 1–2 months as compared to fire emissions from South America and southern Africa shown in Fig. 1 is possibly caused by the seasonality of deep convection, which will be discussed in more detail in Sect. 3.5. Due to poleward transport of polluted southern hemispheric air masses, there is an increase in Antarctic HCN at 8 km from 160 pptv in June to 270 pptv in November/December, followed by a subsequent continuous reduction. The meridional transport time, reflected by the time delay, will be investigated in more detail in Sect. 3.4. The lowest tropospheric northern hemispheric values of 200–250 pptv were observed during January and February and the lowest southern hemispheric HCN amounts of 160–180 pptv during May/June. Possible reasons for the lower southern values are more effective ocean uptake (larger ocean areas) and a shorter biomass burning season. In every latitude band the seasonal variations at 8 km are in good agreement with the variations in the ground-based HCN column amounts in phase and in fairly good agreement in amplitude.

Figure 6. Climatological monthly mean HCN volume mixing ratios measured by MIPAS at the altitudes of 8 (black), 12 (red), 16 (blue) and 20 km (green) in the latitude bands 60–90° (top row), 30–60° (middle row) and 0–30° (bottom row) for the Northern (left column) and Southern Hemisphere (right column). Data are averaged over the time period 2002 to 2012. Black crosses are monthly mean HCN column amounts from ground-based FTIR measurements at the NDACC stations Kiruna (top left), Toronto (middle left), Izaña (bottom left), Arrival Heights (top right) and Lauder (middle right). No ground-based data for the latitude band 0–30° S (bottom right).
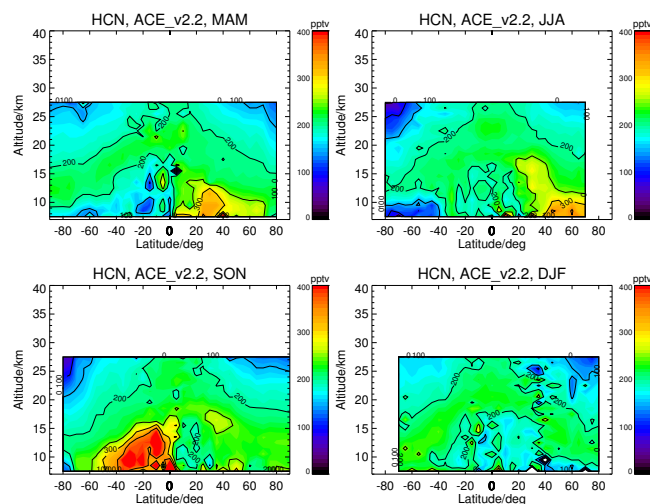
The seasonality at 12 km altitude is slightly weakened but very similar to the variations at 8 km at low latitudes, and due to growing stratospheric contributions is increasingly attenuated at mid- and high latitudes. This effect becomes even stronger at the altitude of 16 km, which is stratospheric in the whole of the extratropics. At 20 km, which is stratospheric at all latitudes, the mid-latitude and tropical HCN amounts are between 230 and 250 pptv and exhibit nearly no seasonal variation. Due to subsidence in the Antarctic vortex, the respective time series from high southern latitudes shows a distinct variation, with minimum values as low as 160 pptv around October. The effect of subsidence is not as clearly visible in the Arctic vortex in boreal winter and spring.

3.3 Comparison with ACE-FTS and with INTEX-B measurements

Figure 7 shows seasonal latitude–height cross sections of HCN amounts (v2.2) measured by ACE-FTS during the years 2004 to 2010, displayed in the same manner as the MIPAS climatology in Fig. 2. The spatial and temporal coverage of ACE-FTS data is considerably lower, which is caused

by the different measuring principle (solar occultation) and the high inclination orbit of SCISAT. Particularly few measurements, restricted to February, April, August and October, were performed in the tropics. At high southern latitudes no measurements were made in February, June, October and December. The background HCN amounts retrieved from ACE-FTS data are generally somewhat lower than those retrieved from MIPAS observations. However, in every season the shape of the HCN distributions observed by ACE-FTS agrees rather well with the respective MIPAS cross sections. During boreal spring, ACE-FTS also observed a plume of comparable size and strength as MIPAS in the northern tropics and subtropics and moderately enhanced HCN amounts at northern mid-latitudes. Similar as in MIPAS HCN, boreal summer is characterised by a plume of large vertical extent inside the Asian monsoon anticyclone and by intensified biomass burning at northern mid- to high latitudes. The highest ACE-FTS HCN amounts were also measured between September and November at southern hemispheric low to mid-latitudes, covering almost exactly the same area as the biomass burning plume observed by MIPAS. Further,
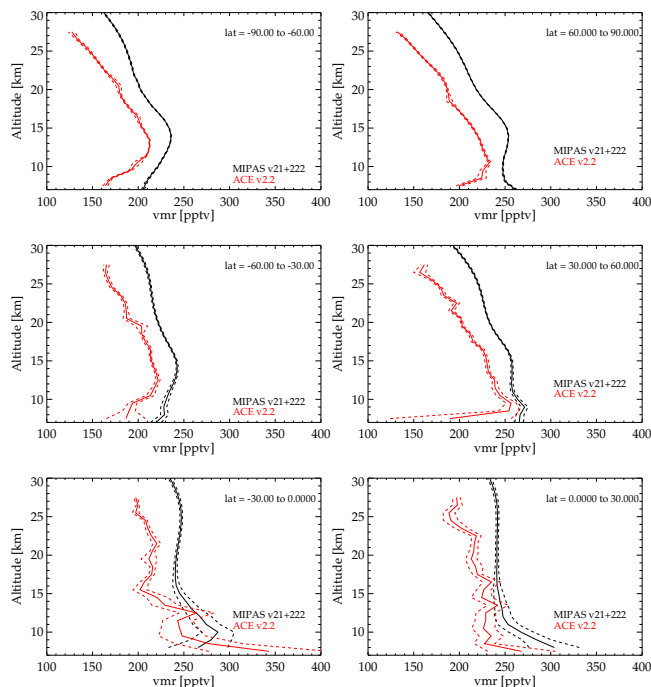
Figure 7. Climatological latitude–height cross sections of HCN volume mixing ratios (v2.2) measured by ACE-FTS during March to May (top left), June to August (top right), September to November (bottom left) and December to February (bottom right). The distributions are averaged over the time period 2004 to 2010.

Figure 8. Mean HCN profiles measured by MIPAS (solid black lines) and by ACE-FTS (v2.2, solid red lines) from ACE-MIPAS matches during the time period 2004–2010 in the latitude bands 60–90° (top row), 30–60° (middle row) and 0–30° (bottom row) in the Southern (left) and Northern Hemisphere (right). Dashed lines are the standard errors of the mean.

ACE-FTS measured a similar seasonality of very low HCN amounts over the tropical and southern oceans. These HCN minima are even lower than those observed by MIPAS. Poleward transport of enhanced HCN during and after the southern hemispheric biomass burning season is also confirmed by the ACE-FTS distributions. The already completed dissolution of the southern hemispheric ACE-FTS plume at southern mid-latitudes in boreal winter, which is different to the MIPAS results, can at least partly be due to sampling issues. In contrast to MIPAS observations, in this region the ACE-FTS distribution is dominated by measurements from January, when the plume is already considerably weaker than in December. HCN climatologies derived from ACE-FTS measurements have already been published by Lupu et al. (2009), Randel et al. (2010) and Park et al. (2013).

As a more quantitative intercomparison, Fig. 8 shows mean HCN profiles from coincident ACE-FTS and MIPAS observations in six different latitude bands. For each ACE-FTS observation, all MIPAS scans inside a radius of 500 km and within a maximum time offset of 5 h were taken into account, resulting in 7104 and 10 397 matching ACE-FTS and MIPAS profiles, respectively. Multiple assignment of one MIPAS profile to different ACE-FTS profiles was not allowed. Then, all selected ACE-FTS and MIPAS profiles of each latitude band were averaged. There is rather good agreement in the shape of the averaged profiles, but the HCN VMRs of MIPAS are slightly higher than the ACE-FTS values. The offset is 10–40 pptv (4–16 %) at 10 km and 40–50 pptv (25–30 %) at 25 km altitude. Larger deviations at the lowermost altitudes are of less significance, because a con-

siderable portion of the matching profiles was truncated further up due, for example, to cloud contamination.

A possible reason for the deviations between the profiles is the use of different spectral bands for retrieval. The spectral regions used for ACE-FTS HCN retrievals are 1395–1460 and 3260–3355 cm^{-1} (Lupu et al., 2009), while for MIPAS retrievals microwindows between 729.5 and 776.95 cm^{-1} were applied. Since the spectroscopic uncertainties of the strongest HCN lines in each of these spectral regions listed in the HITRAN database (Rothman et al., 2013) are 5–10 % both for intensity and pressure broadening, they can lead to a systematic bias of up to 20 %. This could explain most of the differences in Fig. 8.

Figure 9 shows a comparison of MIPAS HCN profiles with airborne in situ HCN measurements performed on the DC-8 aircraft of the National Aeronautics and Space Administration (NASA) during the Intercontinental Chemical Transport Experiment Phase B (INTEX-B) (Singh et al., 2009). The left graph contains the averages of all samples obtained in INTEX-B phase 1, which took place from 4 to 22 March 2006 over the northern Pacific and the western United States, and the right graph the averages of phase 2 performed between 17 April and 15 May 2006 over the southern United States and Mexico. INTEX-B data were obtained from the NASA website (https://www.espo.nasa.gov/
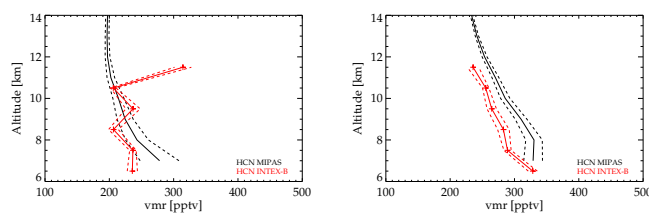
intex-b/). MIPAS profiles are averaged over the respective campaign duration and flight area. Except for the uppermost value at 11.5 km, which exhibits a larger uncertainty and appears to be an outlier, the INTEX-B values between 7.5 and 10.5 km oscillate closely around the MIPAS profile. Thus there is nearly no bias between the two data sets in phase 1. In phase 2 the MIPAS HCN amounts are 25–50 pptv higher, but well within the standard deviation of the INTEX-B data.

On the whole, MIPAS HCN amounts appear to be slightly higher (20–50 pptv) than HCN measurements of ACE-FTS and INTEX-B. Associated uncertainties, however, have only limited implications for the following discussion, focusing on seasonal and interannual variations.
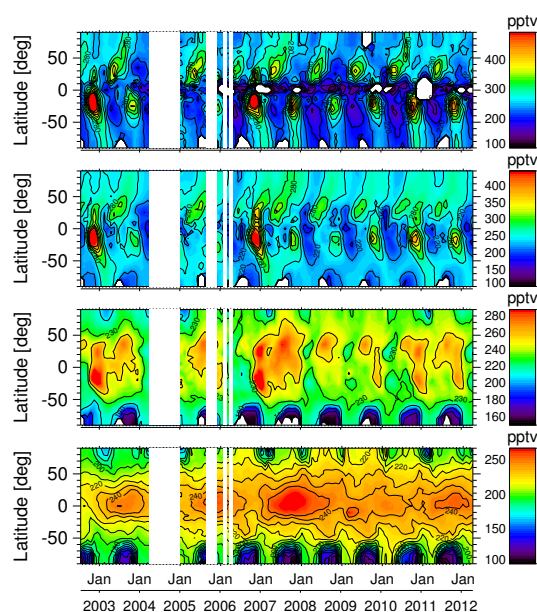
3.4 Time series

To illustrate interannual variations, Fig. 10 shows time versus latitude cross sections of monthly zonal averages of HCN at 10, 14, 18 and 22 km altitude covering the operational period of MIPAS from June 2002 to April 2012. Averaging was performed for 7.5° latitude bins at the poles and 5° latitude bins elsewhere, which generally resulted in adding up of several hundred to more than a thousand values at the altitude of 10 km and above. Only at high latitudes and low altitudes were fewer values binned during winter and spring, e.g. 10–15 values at 10 km. As already shown in Figs. 2 and 3, at 10 and 14 km (top and second row) the most significant signatures of biomass burning are visible in the southern hemispheric tropics and subtropics. In this region the HCN distribution exhibits a clear annual cycle with maxima in October–November somewhat after the peak of southern hemispheric biomass burning and minima during boreal spring. However, the magnitude of these maxima varies considerably between 300 and more than 500 pptv. Especially strong southern hemispheric biomass burning plumes were observed at the end of the years 2002 and 2006 and particularly weak plumes in the years 2003 and 2008 (cf. Sect. 3.5). The cross section at 10 km shows the propagation of enhanced tropospheric HCN to high southern latitudes within ~ 2 months after appearance of the tropical and subtropical HCN maxima. Meridional transport of HCN is the only obvious process to explain this observation, because there are no further sources of HCN at high southern latitudes. Poleward transport of considerable amounts of southern hemispheric biomass burning products has already been shown by Zeng et al. (2012), who discussed time series of ground-based FTIR measurements of CO, HCN and C_2H_6 above Lauder (New Zealand) and Arrival Heights (Antarctica). This transport process is also visible in the ground-based HCN column amounts presented in Fig. 6, which peak above Lauder in October/November and above Arrival Heights in December/January.

Significant signatures of biomass burning also occur in the northern tropical and subtropical troposphere. The underlying period in this region is an annual cycle with

Figure 9. Comparison of MIPAS HCN with airborne in situ measurements of phase 1 (4–22 March 2006, northern Pacific and western US, left) and phase 2 (17 April–15 May 2006, southern US and Mexico, right) of the INTEX-B campaign. INTEX-B HCN data (solid red lines) are sample averages over the flight tracks and MIPAS HCN profiles (solid black lines) are averages over the INTEX-B measurement periods and flight areas. Dashed lines are the standard errors of the mean.
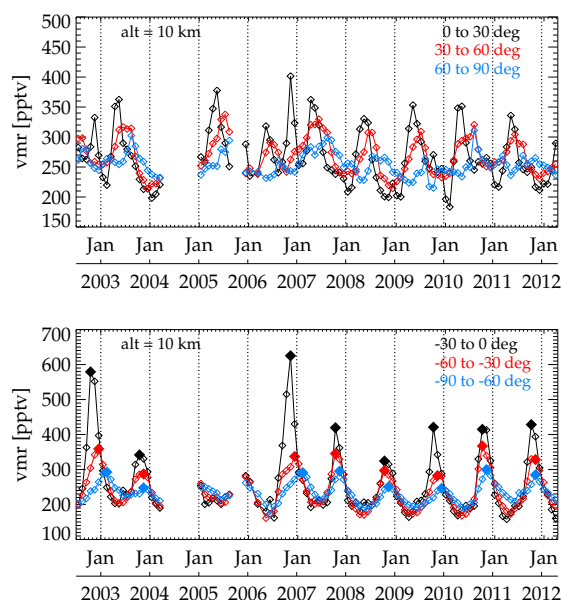
Figure 10. Time series of monthly and zonally averaged HCN measured by MIPAS at 10 km (top panel), 14 km (second panel), 18 km (third panel) and 22 km altitude (bottom panel). White areas extending over the whole latitude range are data gaps due to operational shutdown of MIPAS, white areas after mid-2005 at 10 km in the equatorial region are caused by upward shift of the RR-mode limb scans towards low latitudes, and data gaps at high latitudes are caused by polar stratospheric clouds. Note the different VMR scales.

maxima around May in the tropics, i.e. after and during the biomass burning seasons in northern Africa and in southern Asia. In the northern subtropics maximum HCN amounts appear later around July during the peak of the Asian monsoon period. However, especially at 14 km, there are additional peaks around November 2002, 2006 and 2010 caused by strong biomass burning in Indonesia and by northward effusion from the southern hemispheric plume (cf. Sect. 3.2), leading to semi-annual cycles during

these periods. The reason for intensive burning in Indonesia during the years 2002 and 2006 (cf. Fig. 1) is a strong positive phase of the so-called El Niño–Southern Oscillation (ENSO) (http://www.cpc.ncep.noaa.gov/products/analysis_ monitoring/ensostuff/ensoyears.shtml), characterised by drought periods in this region. These features will be investigated in more detail in Sect. 3.5. Enhanced HCN is obviously also transported to higher northern latitudes, but at 10 km this pattern is not as clear as in the Southern Hemisphere due to additional biomass burning at northern mid-latitudes. A clearer pattern appears at 14 km, showing northward transport of low-latitude upper tropospheric pollution into the extratropical lower stratosphere after breakdown of the AMA (cf. Randel and Jensen, 2013).
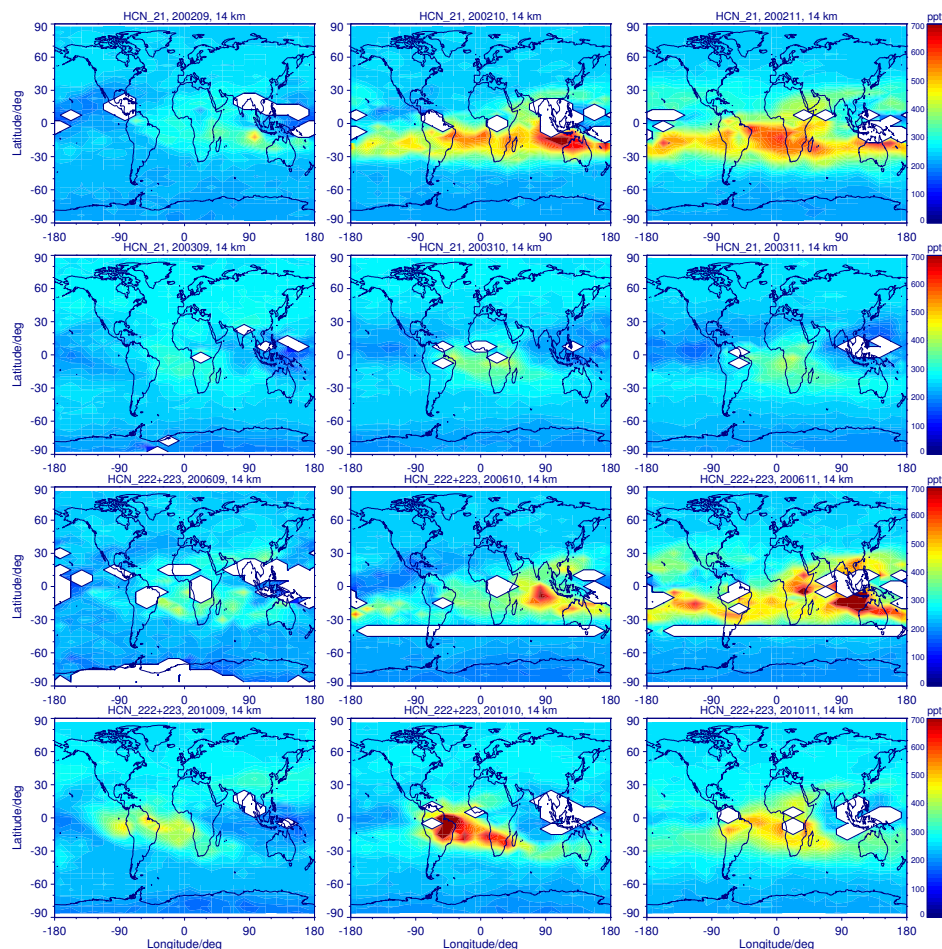
At the altitude of 18 km (third row) most of the annual and semi-annual maxima are still observable, but the amplitudes of the cycles are reduced. The distribution at this altitude gives information about transport of elevated HCN amounts into the stratosphere. The time from the end of 2006 until the end of 2007 was the most effective period, characterised by upward transport of strongly enhanced HCN in the southern hemispheric and Indonesian biomass burning plumes at the end of 2006, above northern Africa in spring 2007 and in the highly polluted AMA during summer 2007 (see Sect. 3.5). The combination of the same four sources is also responsible for the features of elevated HCN observed from the end of 2002 until the end of 2003 (see Sect. 3.5). High HCN amounts observed from mid-2010 until the end of 2011 resulted from upward transport in the two consecutive AMAs and from intensive South American biomass burning in 2010 (see Sect. 3.5). Due to ordinary biomass burning only (no El Niño year and no outstanding biomass burning in South America), lower amounts of HCN were observed in the tropical and subtropical lowermost stratosphere during the period 2008 to mid-2010. Tropical HCN at 22 km altitude (bottom row) exhibits longer periodicities of 2 and 4 years with maxima from the beginning of 2003 to 2004, from mid-2005 to mid-2006, from early 2007 to autumn 2008 and from 2011 to 2012. These maxima appear to be accumulations of the consecutive pulses at the altitudes below. The time delay of their appearance compared to the maxima at 18 km confirms upward transport into the stratosphere. In general, entry of enhanced HCN into the lower stratosphere seems to be somewhat more effective in the Northern than in the Southern Hemisphere, but the dominance of the Asian monsoon is not as distinct as shown by Randel et al. (2010, Fig. 3). This finding also persists after averaging of MIPAS HCN over the altitude region 16–23 km as performed by those authors. However the longer time series of MIPAS contains a larger portion of periods in which the contributions from the southern hemisphere were larger than during the timeframe 2004–2009 observed by Randel et al. (2010).

For better quantification of meridional transport times in the upper troposphere, Fig. 11 shows monthly zonal averages of HCN VMRs at 10 km altitude for the latitude bands

Figure 11. Top: time series of monthly mean HCN measured by MIPAS at 10 km altitude in the latitude bands 0–30° N (black), 30–60° N (red) and 60–90° N (blue). Bottom: same as top but for the latitude bands 0–30° S (black), 30–60° S (red) and 60–90° S (blue). Solid symbols indicate maxima of the respective latitude band.

0–30°, 30–60 and 60–90°, both for the Northern and Southern Hemisphere. In the Southern Hemisphere there is a rather clear transport pattern, which becomes evident in the time lags between the curves from low and high latitudes. Meridional transport times can be estimated from the shifts between the HCN maxima at southern tropical, mid-latitude and polar latitudes (solid black, red and blue symbols). In most years the shifts between the tropics and high latitudes amount to 1 month, but in 2006/2007 they amount to 3 months and in 2002/2003 to 4 months (cf. Table 1). The average value of all years is ∼ 1.8 months. The shifts between mid- and high latitudes, as expected, are shorter, namely 1 month on average. Consistent time lags of 1–2 months between the low-, mid- and high-latitude southern hemispheric maxima at 8 km are also visible in the seasonal climatology in Fig. 6. For comparison, the transport time between Lauder (New Zealand, 45.0° S) and Arrival Heights (Antarctica, 77.8° S) derived by Morgenstern et al. (2012) from correlation analysis of FTIR CO column amounts is 15–40 days. Poleward transport times at 10 km can not be estimated by such a simple approach by MIPAS data of the Northern Hemisphere due to additional biomass burning at midlatitudes and semi-annual variations (Fig. 11, top).

Figure 12. Global distributions of HCN measured by MIPAS at 14 km altitude during September, October and November (left to right) 2002 (top row), 2003 (second row), 2006 (third row) and 2010 (bottom row). White areas contain no measurements due to cloud contamination or discontinuities in the scan pattern (horizontal stripe).

3.5   Reasons for interannual variations

3.5.1   Variations in southern hemispheric biomass burning

To investigate the reasons for interannual variations in the strength of the southern hemispheric maxima in more detail, we compare global HCN distributions of September, October and November of four different years at 14 km altitude (Fig. 12). Averaging was performed for $7.5° \times 15°$ latitude–longitude bins at the poles and $5° \times 15°$ latitude–longitude bins elsewhere.

In each of the 4 years, the southern hemispheric plume is weaker in September than in October and November, although the GFEDv3 fire emissions from southern hemispheric Africa and from South America peak in August/September (see Fig. 1). A possible reason for this time offset is a delay in effective lifting until the onset of deep convection, which occurs above the fire emission areas later in the year towards austral summer. This is illustrated by the

southern hemispheric OLR of August and November 2002 provided by NOAA/ESRL (Fig. 4, bottom). In August 2002 there are no high clouds (OLR $\leq 220\,\mathrm{W\,m^{-2}}$) above Brazil and southern hemispheric Africa, while in November 2002 deep convection has moved considerably southward above the fire regions. The delay between fire emissions and lofting of pollutants into the upper troposphere, caused by meridional movement of the convection zones, has already been described by Liu et al. (2010, 2013, and references therein).

The upper row of Fig. 12 shows the development of the extensive plume of the year 2002. In September, enhanced HCN amounts between 300 and 400 pptv were observed in an area extending from Brazil over southern Africa towards Australia. In October, considerably higher HCN amounts of up to more than 700 pptv were measured above northern Australia and Indonesia. Enhanced HCN values then covered the whole southern tropical and subtropical latitude band, especially above the southern tropical Atlantic. The high HCN amounts above Indonesia are consistent with strong

Table 1. Time shift between HCN maxima in the latitude bands 0–30 and 60–90° S and between maxima in the bands 30–60 and 60–90° S. Time shifts are given in months for the altitude of 10 km and for the different years of the operational period of MIPAS. Due to data gaps, time shifts could not be derived for the years 2004 and 2005.

Year	Time shift 0–30° to 60–90° S [months]	Time shift 30–60° to 60–90° S [months]
2002	4	2
2003	1	0
2004	–	–
2005	–	–
2006	3	2
2007	1	1
2008	1	1
2009	2	1
2010	1	1
2011	1	0

GFEDv3 fire emissions in this region peaking in September (cf. Fig. 1). The strong plume in November centred between South America and southern Africa and extending towards Australia and the southern Pacific was caused by biomass burning in South America and southern and central Africa during the preceding months (cf. Fig. 1). In each of the three months a certain part of the pollutants was transported above northern Africa and the northern Indian Ocean towards southern Asia. Thus, the contiguous area of enhanced HCN extending from the southern subtropics over the Equator and into the northern subtropics in the time series in Fig. 10 was caused by sources in South America, southern Africa and additionally strong biomass burning in Indonesia.

In 2003 MIPAS observed one of the weakest plumes of its measurement period (Fig. 12, second row). Maximum HCN amounts did not exceed 400 pptv, and values above 330 pptv were measured above the southern tropical and subtropical Atlantic, southern Africa and parts of the Indian Ocean only. In this year no biomass burning signatures from Indonesia and Australia were detected. Instead, the HCN amounts above Indonesia and the tropical Pacific amounted to 200 pptv only or even less. Low HCN amounts above Indonesia are consistent with only little fire emissions from equatorial Asia in the GFEDv3 database (Fig. 1). While fire emissions from southern Africa were in the normal range, rather low emissions from South America are the second reason for the weak plume in 2003 (Fig. 1). A comparably weak plume was observed in 2008 (cf. Fig. 10), when South American and Indonesian fire emissions were also low.

Another very strong southern hemispheric HCN plume was detected in the year 2006 (Fig. 12, third row). In October, the highest HCN amounts were observed around In-
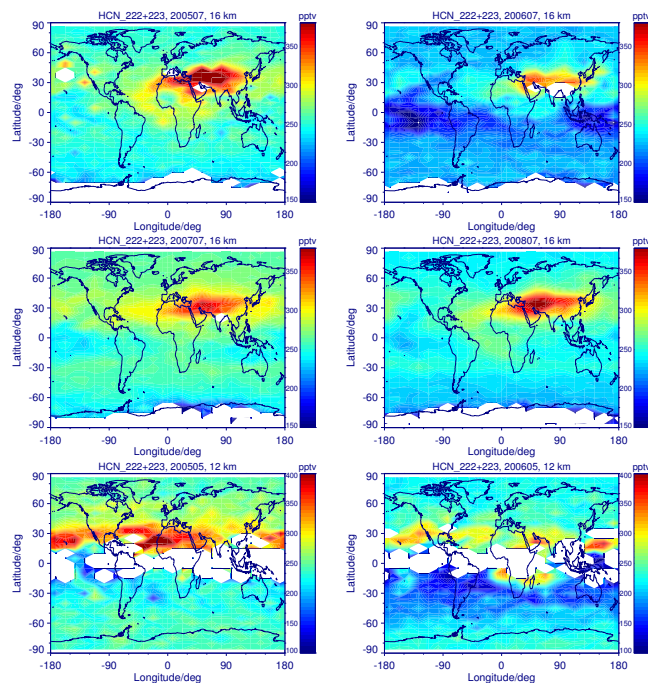
donesia and above the Indian Ocean. This feature is in good agreement with the CO distribution obtained by MLS during the same month at the 147 hPa level (~ 14 km) (Liu et al., 2013, Fig. 8b). In November there was an even more distinct maximum above and around Indonesia, extending considerably into the Northern Hemisphere, and another "hotspot" above eastern Africa. The huge Indonesian maximum is consistent with very high GFEDv3 fire carbon emissions from equatorial Asia peaking in October 2006 (Fig. 1). Amplified by additional contributions from southern Africa and South America, there were strongly enhanced HCN amounts in the whole subtropical latitude band. Thus, like in 2002, overlap of emissions from Indonesia, Africa and South America led to a region of strongly enhanced HCN, extending from southern mid-latitudes to the northern subtropics in late 2006.

The year 2010 was characterised by rather distinct signatures of biomass burning above the southern Atlantic and west of Peru as early as in September (Fig. 12, bottom row). During October this plume became very strong, and enhanced HCN extended from Brazil to southern Africa with effusion towards Australia as well as to northern Africa. These high HCN amounts were caused by very intensive fire emissions from Brazil during August and September (cf. Fig. 1), which were transported into the upper troposphere by deep convection reaching the fire region somewhat later in the year (see Fig. 4, bottom row). The HCN distribution of October 2010 is in very good agreement with CO measurements of MLS at the 147 hPa level (Liu et al., 2013, Fig. 8d). Referring to publications of Chen et al. (2011), Fernandes et al. (2011) and Lewis et al. (2011), these authors identify the severe drought in South America in 2010 as a reason for the enhanced fire activity. The drought resulted from a strong El Niño in 2009 and early 2010 and from a very warm tropical North Atlantic in 2010. In November the plume had somewhat diluted and dispersed over the whole southern subtropical latitude band and to a minor part over southern Asia and the northern subtropics. In this year no significant biomass burning signatures were detected above Indonesia, which is consistent with missing fire emissions from equatorial Asia in Fig. 1.

Thus, the extraordinarily strong southern hemispheric plumes observed in 2002 and 2006, also affecting the northern tropics and subtropics, were caused by overlap of biomass burning in South America, southern Africa and additionally high emissions from Indonesia. The strong plume of the year 2010 resulted from biomass burning far above average in South America.

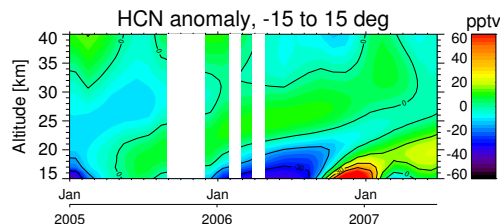### 3.5.2 HCN in the Asian monsoon anticyclone

The AMA is a meteorological feature which regularly develops in the upper troposphere over southern Asia during the summer monsoon in June, July and August. It is a reservoir of air masses in which pollutants from the northern subtropics are trapped and transported high into the UTLS re-

Figure 13. Global HCN distributions measured by MIPAS at 16 km altitude during the peak of the Asian monsoon in July 2005 and 2006 (top row) and July 2007 and 2008 (middle row), and HCN distributions measured at 12 km in May 2005 and 2006 (bottom row).

Figure 14. Time series of monthly averaged HCN measured by MIPAS in the latitude band 15° S–15° N from January 2005 to June 2007. The average HCN VMR of each altitude has been subtracted. White areas are data gaps.

gion (Randel et al., 2010, and references therein). The HCN amounts measured by MIPAS inside the AMA are generally more regular than in the southern hemispheric biomass burning plume, but also exhibit interannual variations. To illustrate this, we show distributions at 16 km altitude of the consecutive years 2005–2008.

In July 2005 (Fig. 13, top left), HCN VMRs of up to 400 pptv were measured in the complete region covered by the central part of the anticyclone from the western Mediterranean Sea to eastern Asia. Enhanced HCN amounts were also observed further west in the outskirts of the AMA above the mid-Atlantic (cf. Fig. 5, bottom), indicating possible outflow into the tropics. The area covered by enhanced HCN in July 2005 is in good agreement with MLS observations of increased CO at 100 hPa ($\sim$ 16.5 km) (Liu et al., 2013, Fig. 5). In July 2007 and 2008 (middle row) the AMA contained nearly as high amounts of HCN as in 2005, extending over approximately the same area. In both years there is also indication of southwestward outflow towards the tropical Atlantic, which is a potential additional source of a tropical HCN tape recorder. However, in July 2006 maximum HCN amounts in the AMA were 300–350 pptv only, restricted to the area between the Middle East and China (top right). A similar interannual variation in the HCN amounts inside the AMA was observed by ACE-FTS and MLS (Randel et al., 2010, Fig. 3). Since the HCN VMRs at 16 km were globally lower in July 2006 than in the other years
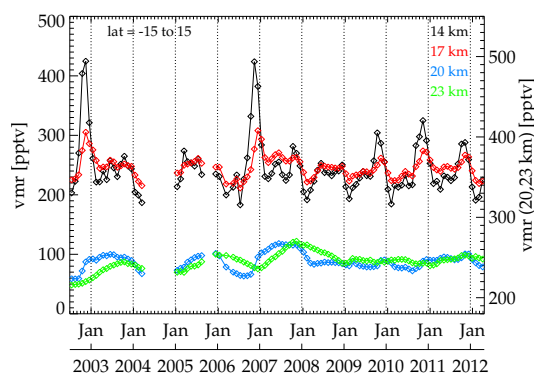
shown, we assume release of less HCN into the northern tropics and subtropics as reason for the more weakly polluted AMA in 2006. This is confirmed by global distributions at 12 km altitude (bottom row), which show considerably lower HCN amounts in the northern subtropical band in May 2006 than in May 2005. Substantial differences in the intensity of South and Southeast Asian biomass burning between the years 2005 and 2006 are consistent with HCN emission fluxes calculated by Lupu et al. (2009, Fig. 1) from the GFEDv2 biomass burning inventory, which were much higher in early 2005 than in early 2006.

3.6 The tropical HCN tape recorder

As outlined in Sect. 1, a tropical tape recorder signal was found in MLS and ACE-FTS HCN data by Pumphrey et al. (2008). They detected a stratospheric cycle of 2 years in the latitude band 15° S–15° N for the time period mid-2004 to mid-2007. Subsequent analyses and model calculations, which have been briefly discussed in Sect. 1, mostly resulted in biennial periodicities, but, for instance, Pommrich et al. (2010) postulated an irregular cycle over a longer time period. Thus the question of the dominant period, if any, in the HCN tape recorder signal is not yet fully answered and the long time series of MIPAS data can help to solve the problem.

First of all we checked whether the signal derived by Pumphrey et al. (2008) can also be found in MIPAS data. The results of this test are presented in Fig. 14, which contains the MIPAS HCN "tape recorder signature" for the period 2005 to mid-2007 and the latitude band 15° S–15° N. The mean values of the period were subtracted for each retrieval altitude and a 3-month running mean was applied. There is good agreement with the tape recorder signals derived from ACE-FTS and MLS HCN data (cf. Pumphrey et al., 2008, Fig. 1) in phase as well as in magnitude. However, Fig. 10 shows that the period 2005–2007 is not representative of the whole inner tropical HCN data set of MIPAS, because it exhibits an extraordinarily strong upper tropospheric maximum at the end of 2006 caused by southern hemispheric and additional intensive biomass burning in Indonesia. On the other
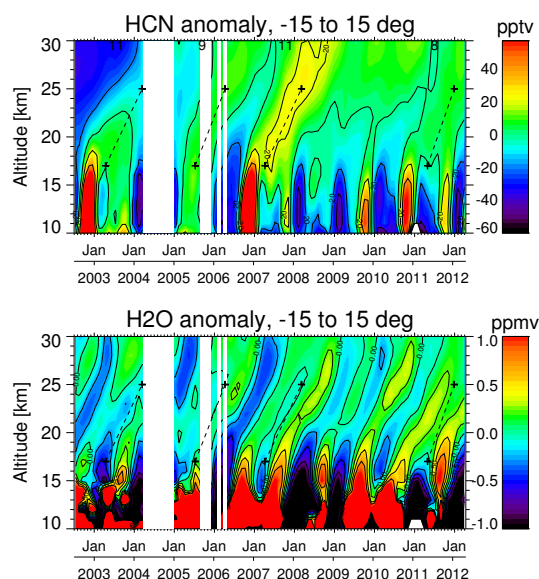
Figure 15. Time series of monthly mean HCN measured by MIPAS at 14 (black), 17 (red), 20 (blue) and 23 km altitude (green), zonally averaged over the latitude band 15° S–15° N. For more clarity, the values at 20 and 23 km altitude are related to the right y axis.

hand, the northern tropical HCN maximum around May 2006 is nearly completely missing. The subsequent years 2008–2009 exhibit a more regular pattern with alternating northern maxima around May and southern maxima around October–November.

For further illustration of the situation at tropical latitudes, Fig. 15 shows time series of monthly mean HCN at 14, 17, 20 and 23 km altitude, zonally averaged over the latitude band 15° S–15° N. The most prominent signatures at 14 km are the strong maxima in November 2002 and 2006 caused by overlap of biomass burning in the Southern Hemisphere with additional contributions from Indonesia, followed by the maxima at the end of 2009, 2010 and 2011. Accordingly, the dominant period is an annual cycle with maxima in November. But there are also regular, generally weaker maxima around April to May resulting from biomass burning in the Northern Hemisphere, which cause an overlapping semi-annual cycle. At 17 km altitude the November maxima are considerably reduced, but the periodicities are generally the same as at 14 km. The time lag between the maxima at 14 and 17 km is 0–1 months only. For comparison, the time delays between MLS CO maxima at 147 and 68 hPa (about 14.3 and 19 km altitude) published by Liu et al. (2013) are 0–2 months for northern hemispheric fires and 3–4 months for southern hemispheric fires. At 20 km altitude the amplitude of the variations is further reduced and the periodicities are longer. Between 2002 and 2007 there is an approximately biennial cycle with three relatively strong maxima centred at mid-2003, at the end of 2005 and around mid-2007, which are much broader than the maxima at the lower altitudes. The following time period exhibits only weak and generally more short-lived maxima mainly at the end of the years. At 23 km altitude the strong maxima of the time period 2003 to 2007 reappear temporally delayed by about 4 months, indicating upward transport.

For better visualisation of a tape recorder signal in the whole MIPAS HCN data set, Fig. 16 (top) shows a time-

Figure 16. Top: time series of monthly averaged HCN measured by MIPAS in the latitude band 15° S–15° N from July 2002 to April 2012. The average HCN VMR of each altitude has been subtracted. Dashed lines indicate the vertical slope of the positive anomalies. The numbers at the top are the time delays in months for transport of the positive anomalies from 17 to 25 km altitude. Bottom: same as top but for MIPAS H_2O. Dashed lines are the HCN slopes for comparison of ascent speeds.

height cross section of the inner tropics (15° S–15° N) from July 2002 to April 2012 after subtraction of the average value at each altitude and application of a 3-month running mean. For comparison with another tropospheric tracer, the water vapour tape recorder signal derived from MIPAS measurements is also shown (Fig. 16, bottom). Like in Fig. 15, the upper tropospheric (10–17 km) HCN anomaly exhibits semi-annual and annual cycles of considerably varying strength and a fast upward propagation. A stratospheric tape recorder signal is visible in four broad positive and negative anomalies and additionally one rather weak positive band. Vertical transport times in the lower stratosphere are considerably longer. The time shifts for the distance between 17 and 25 km altitude, indicated by the dashed lines and the numbers in Fig. 16 (top), are 8–11 months. These values are in good agreement with the vertical velocity of 0.02–0.04 cm s^{-1} for the H_2O tape recorder signal published by Mote et al. (1996) for the altitude region 16–32 km, which results in a time delay of 10 months between 17 and 25 km (for 0.03 cm s^{-1}). Further, there is also good agreement with the H_2O tape recorder signatures in Schoeberl et al. (2008, Fig. 6a).

Due to lower interannual variations in the H_2O amounts at the tropopause, the stratospheric H_2O tape recorder signal (Fig. 16, bottom) exhibits a rather regular annual cycle (cf. Mote et al., 1996; Schoeberl et al., 2008). For a cross check of vertical velocities, the upward propagation of the
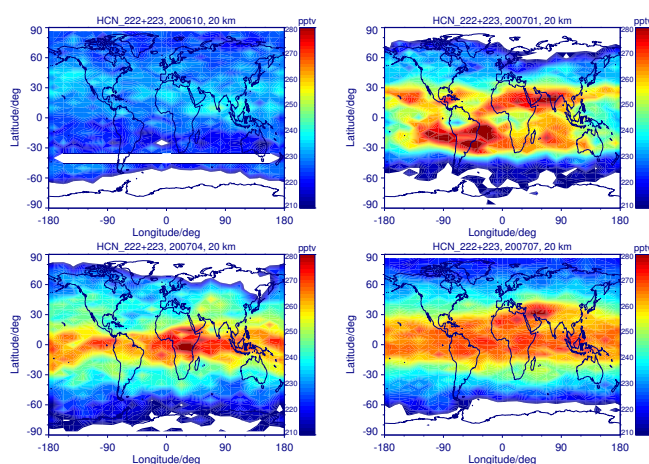
HCN tape recorder anomalies estimated in Fig. 16 (top) is overplotted. It is evident that, apart from the different tape recorder periods, the upward velocities agree quite well.

The first band of enhanced HCN entering the stratosphere covers the time period from the end of 2002 to end of 2003 at the tropopause and reaches the altitude of 25 km about 11 months later. The second positive anomaly leads from the uppermost troposphere in mid-2005 to the mid-stratosphere in mid-2006. The next band of enhanced stratospheric HCN is the strongest positive tape recorder signal observed in MIPAS HCN and extends from autumn 2006 to the end of 2007 at 17 km and from mid-2007 to the end of 2008 at 25 km altitude. Subsequently, a period follows with mainly depleted HCN at the tropopause and above from the beginning of 2008 until boreal autumn 2010, which is only interrupted by a weak pulse at the end of 2009. The last period of enhanced stratospheric HCN lasts from autumn 2010 to the end of 2011 at 17 km altitude and from autumn 2011 to the end of the observation period at 25 km altitude.

Thus, the stratospheric HCN anomaly exhibits two consecutive biennial cycles with maxima in the lowermost stratosphere centred in mid-2003, mid-2005 and mid-2007 and, apart from the weak signal in 2009, another maximum following in mid-2011. Besides conformity with Pumphrey et al. (2008), the sequence of positive and negative anomalies starting at the tropopause between mid-2005 and mid-2007 is in good agreement with the ACE-FTS HCN tape recorder signal presented in Park et al. (2013, Fig. 14) for the latitude band 10° S to 30° N and with tropical HCN anomalies of the GEOS-Chem model presented by Li et al. (2009, Fig. 6).

The starting times of the first, third and last positive anomaly at the tropopause (end of 2002, 2006 and 2010) indicate that they were initiated by the intensive biomass burning in boreal autumn prevailing in these years, in 2002 and 2006 resulting from accumulation of southern hemispheric and strong Indonesian fire emissions and in 2010 from extraordinarily strong emissions from Brazil (see Figs. 1, 12). However, their long duration hints at overlap with subsequent contributions from biomass burning in tropical Africa and outflow from the AMA. The onset of the second anomaly at the tropopause in spring 2005 and its relatively short duration suggest that it was caused by springtime biomass burning in northern Africa and Asia and by the effusion from the highly polluted AMA of 2005. In summary, we think the apparent biennial cycle is caused by interannual variations in biomass burning and does not have a direct meteorological reason beyond the effect of meteorology on the biomass burning itself. This assumption is corroborated by GEOS-Chem model calculations of Li et al. (2009), who found that the interannual differences of HCN amounts in the tropical troposphere and lower stratosphere are much more strongly controlled by variations in biomass burning than by the meteorology.

The supply of enhanced HCN from different regions leading to the strong tape recorder signal of 2007 is illustrated in Fig. 17 by distributions at 20 km altitude. In October 2006

Figure 17. Global HCN distributions measured by MIPAS at 20 km altitude during October 2006 (top left), January 2007 (top right), April 2007 (bottom left) and July 2007 (bottom right).

(top left), fresh pollution has not yet reached this high altitude and the HCN amounts in the whole southern tropical and subtropical latitude band amount to about 220 pptv. The somewhat higher HCN amounts in the northern tropics and subtropics presumably originate from the previous summer's AMA. In January 2007 (top right), large tropical areas contain enhanced HCN amounts of up to 280 pptv which have been released by southern hemispheric and Indonesian biomass burning. After a decrease in February and March 2007 (not shown), enhanced HCN, refreshed by biomass burning in central Africa, covers the whole tropical latitude band in April 2007 (bottom left). Due to polluted air masses flowing out from the AMA, the tropical band of enhanced HCN still exists in July 2007 (bottom right) and reaches further northwards than in April.

4 Conclusions

We have presented a climatology of MIPAS HCN data, covering the period June 2002 to April 2012, with the main focus on the tropical and subtropical upper troposphere and lower stratosphere. HCN is a nearly unambiguous tracer of biomass burning with a tropospheric lifetime of 5–6 months, which is short enough to observe seasonal and annual differences in fire activity, but sufficiently long to study long-range and vertical transport. The highest upper tropospheric HCN amounts were detected in boreal autumn in the southern hemispheric tropics and subtropics in a large plume extending up to 17 km altitude. Highest northern hemispheric HCN amounts were measured in boreal summer in the subtropics and at midlatitudes. The large subtropical plume extending up to 18 km altitude is caused by trapping of pollutants inside the Asian monsoon anticyclone. MIPAS HCN data also indicate effusion of air masses in the UTLS region from the Asian mon-

soon anticyclone to the inner tropics, but they do not show such a predominance of the Asian monsoon anticyclone as a source of stratospheric HCN as found by Randel et al. (2010) from analysis of ACE-FTS and MLS data. A third distinct plume was observed above northern Africa in boreal spring. Possibly due to ocean uptake (Li et al., 2000, 2003; Singh et al., 2003), the tropospheric HCN amounts exhibit minima above the tropical and subtropical oceans, which are most pronounced during boreal winter and spring. There is generally good agreement with the HCN climatology obtained from spaceborne ACE-FTS measurements and with airborne in situ data from the INTEX-B campaign. However, MIPAS HCN data are higher by about 10–50 pptv than the ACE-FTS and INTEX-B values.

Time series of upper tropospheric HCN data show a regular annual period of southern hemispheric biomass burning with maxima in October/November. According to the GFED database (van der Werf et al., 2006, 2010), carbon fire emissions from South America and southern Africa peak somewhat earlier in August/September. Distributions of the outgoing longwave radiation provided by NOAA/ESRL indicate that the reason for the time lag of the HCN maxima is probably the delayed onset of deep convection, which becomes more effective in October/November. The influence of the movement of deep convection on the upward transport of pollutants has already been discussed by Liu et al. (2010, 2013). Due to varying burning activities, the size and strength of the southern hemispheric plume exhibit distinct interannual variations with, for example, maximum monthly mean VMRs at 14 km ranging between 400 and more than 700 pptv. MIPAS HCN distributions indicate that the strong plumes of 2002 and 2006 were created by overlap of biomass burning in South America and southern Africa with high additional emissions from Indonesia, and that the plume of 2010 was caused by extraordinarily high fire emissions from Brazil. These observations are confirmed by fire emissions of the GFED database. The fundamental period at northern low to mid-latitudes is also an annual cycle, which in the tropics peaks in April/May during and after the southern Asian and northern African biomass burning season and in the subtropics around July due to trapping of pollutants in the Asian monsoon anticyclone. In several years this cycle is considerably disturbed, either by additional maxima in boreal autumn 2002, 2006 and 2010 resulting from biomass burning in Indonesia and in the Southern Hemisphere or by nearly complete absence of the springtime maximum like in 2006. Enhanced HCN released by tropical and subtropical biomass burning is subsequently transported to high latitudes. The average transport time at 10 km from southern hemispheric low and mid-latitudes to high latitudes is 1.8 months and 1 month, respectively.

The apparently biennial HCN tape recorder signal in the tropical stratosphere derived by Pumphrey et al. (2008) from MLS and ACE-FTS data of the time period mid-2004 to mid-2007 is corroborated by MIPAS data of this period. In the whole MIPAS data set, annual or semi-annual cycles prevail in the tropical upper troposphere due to overlapping signatures from the Northern and Southern Hemisphere, while variations in the lower stratosphere exhibit periodicities of 2 and 4 years. These periodicities, however, do not have a direct meteorological reason but are rather introduced by the interannual variations in biomass burning as already outlined by Pommrich et al. (2010). The broad positive anomalies starting at the tropical tropopause in 2003, 2007 and 2011 are due to contributions from strong southern hemispheric and Indonesian biomass burning in boreal autumn and from northern tropical Africa and the AMA in subsequent boreal spring and summer. The positive anomaly of 2005 seems to be caused by northern hemispheric emissions during boreal spring followed by release from the AMA. Vertical transport of the anomalies is rather fast in the upper troposphere but considerably slower in the stratosphere, e.g. 0–1 months from 14 to 17 km and about 9 months from 17 to 25 km altitude, which is consistent with results from previous studies.

Edited by: P. Haynes

References

Akagi, S. K., Yokelson, R. J., Wiedinmyer, C., Alvarado, M. J., Reid, J. S., Karl, T., Crounse, J. D., and Wennberg, P. O.: Emission factors for open and domestic biomass burning for use in atmospheric models, Atmos. Chem. Phys., 11, 4039–4072, doi:10.5194/acp-11-4039-2011, 2011.

Andrews, A. E., Boering, K. A., Daube, B. C., Wofsy, S. C., Hintsa, E. J., Weinstock, E. M., and Bui, T. P.: Empirical age spectra for the lower tropical stratosphere from in situ observa-

tions of CO$_2$: implications for stratospheric transport, J. Geophys. Res., 104, 26581–26595, 1999.

Bernath, P. F., McElroy, C. T., Abrams, M. C., Boone, C. D., Butler, M., Camy-Peyret, C., Carleer, M., Clerbaux, C., Coheur, P.-F., Colin, R., DeCola, P., De Mazière, M., Drummond, J. R., Dufour, D., Evans, W. F. J, Fast, H., Fussen, D., Gilbert, K., Jennings, D. E., Llewellyn, E. J., Lowe, R. P., Mahieu, E., McConnell, J. C., McHugh, M., McLeod, S. D., Michaud, R., Midwinter, C., Nassar, R., Nichitiu, F., Nowlan, C., Rinsland, C. P., Rochon, Y. J., Rowlands, N., Semeniuk, K., Simon, P., Skelton, R., Sloan, J. J., Soucy, M.-A., Strong, K., Tremblay, P., Turnbull, D., Walker, K. A., Walkty, I., Wardle, D. A., Wehrle, V., Zander, R. and Zou, J.: Atmospheric Chemistry Experiment (ACE): Mission overview, Geophys. Res. Lett., 32, 15, L15S01, doi:10.1029/2005GL022386, 2005.

Boone, C. D., Nassar, R., Walker, K. A., Rochon, Y., McLeod, S. D., Rinsland, C. P. and Bernath, P. F.: Retrievals for the atmospheric chemistry experiment Fourier–transform spectrometer, Appl. Opt., 44, 33, 7218–7231, 2005.

Chen, Y., Randerson, J. T., Morton, D. C., DeFries, R. S., Collatz, G. J., Kasibhatla, P. S., Giglio, L., Jin, Y. F., and Marlier, M. E.: Forecasting fire season severity in South America using sea surface temperature anomalies, Science, 334, 787–791, doi:10.1126/science.1209472, 2011.

Cicerone, R. J. and Zellner, R.: The atmospheric chemistry of hydrogen cyanide (HCN), J. Geophys. Res., 88, 10689–10696, 1983.

Coffey, M. T., Mankin, W. G., and Cicerone, R. J.: Spectroscopic detection of stratospheric hydrogen cyanide, Science, 214, 333–335, 1981.

Edwards, D. P., Emmons, L. K., Gille, J. C., Chu, A., Attié, J.-L., Giglio, L., Wood, S. W., Haywood, J., Deeter, M. N., Massie, S. T., Ziskin, D. C., and Drummond, J. R.: Satellite-observed pollution from Southern Hemisphere biomass burning, J. Geophys. Res., 111, D14312, doi:10.1029/2005JD006655, 2006.

European Space Agency (ESA): Envisat, MIPAS An instrument for atmospheric chemistry and climate research, ESA Publications Division, ESTEC, P.O. Box 299, 2200 AG Noordwijk, The Netherlands, SP-1229, 2000.

Fernandes, K., Baethgen, W., Bernardes, S., DeFries, R., DeWitt, D. G., Goddard, L., Lavado, W., Lee, D. E., Padoch, C., Pinedo-Vasquez, M., and Uriarte, M.: North Tropical Atlantic influence on western Amazon fire season variability, Geophys. Res. Lett., 38, L12701, doi:10.1029/2011gl047392, 2011.

Fischer, H., Birk, M., Blom, C., Carli, B., Carlotti, M., von Clarmann, T., Delbouille, L., Dudhia, A., Ehhalt, D., Endemann, M., Flaud, J. M., Gessner, R., Kleinert, A., Koopman, R., Langen, J., López-Puertas, M., Mosner, P., Nett, H., Oelhaf, H., Perron, G., Remedios, J., Ridolfi, M., Stiller, G., and Zander, R.: MIPAS: an instrument for atmospheric and climate research, Atmos. Chem. Phys., 8, 2151–2188, doi:10.5194/acp-8-2151-2008, 2008.

Glatthor, N., von Clarmann, T., Stiller, G. P., Funke, B., Koukouli, M. E., Fischer, H., Grabowski, U., Höpfner, M., Kellmann, S., and Linden, A.: Large-scale upper tropospheric pollution observed by MIPAS HCN and C$_2$H$_6$ global distributions, Atmos. Chem. Phys., 9, 9619–9634, doi:10.5194/acp-9-9619-2009, 2009.

Holton, J. R., Haynes, P. H., McIntyre, M. E., Douglass, A. R., Rood, R. B., and Pfister, L.: Stratosphere–troposphere exchange, Rev. Geophys., 33, 403–439, 1995.

Höpfner, M., von Clarmann, T., Fischer, H., Glatthor, N., Grabowski, U., Kellmann, S., Kiefer, M., Linden, A., Mengistu Tsidu, G., Milz, M., Steck, T., Stiller, G. P., Wang, D.-Y., and Funke, B.: First spaceborne observations of Antarctic stratospheric ClONO$_2$ recovery: austral spring 2002, J. Geophys. Res., 109, D11308, doi:10.1029/2004JD004609, 2004.

Hsu, N. C., Herman, J. R., and Tsay, S.-C.: Radiative impacts from biomass burning in the presence of clouds during boreal spring in southeast Asia, Geophys. Res. Lett., 30, 1224, doi:10.1029/2002GL016485, 2003.

Kalnay, E., Kanamitsu, M., Kistler, R.,Collins, W., Deaven, D., Gandin, L., Iredell, M., Saha, S., White, G., Woollen, J., Zhu, Y., Chelliah, M., Ebisuzaki, W., Higgins, W., Janowiak, J., Mo, K. C., Ropelewski, C., Wang, J., Leetmaa, A., Reynolds, R., Jenne, R., and Joseph ,D.: The NCEP/NCAR 40-Year Reanalysis Project, B. Am. Meteor. Soc., 77, 437–471, 1996.

Lewis, S. L., Brando, P. M., Phillips, O. L., van der Heijden, G. M. F., and Nepstad, D.: The 2010 Amazon drought, Science, 331, 554–554, doi:10.1126/science.1200807, 2011.

Liebmann, B., and Smith, C. A.: Description of a Complete (Interpolated) Outgoing Longwave Radiation Dataset, B. Am. Meteor. Soc., 77, 1275–1277, 1996.

Li, Q., Jacob, D. J., Bey, I., Yantosca, R. M., Zhao, Y., Kondo, Y., and Notholt, J.: Atmospheric hydrogen cyanide (HCN): biomass burning source, ocean sink?, Geophys. Res. Lett., 27, 357–360, 2000.

Li, Q., Jacob, D. J., Yantosca, R. M., Heald, C. L., Singh, H. B., Koike, M., Zhao, Y., Sachse, G. W., and Streets, D. G.: A global three-dimensional model analysis of the atmospheric budgets of HCN and CH$_3$CN: constraints from aircraft and ground measurements, J. Geophys. Res., 108, 8827, doi:10.1029/2002JD003075, 2003.

Li, Q., Palmer, P. I., Pumphrey, H. C., Bernath, P., and Mahieu, E.: What drives the observed variability of HCN in the troposphere and lower stratosphere?, Atmos. Chem. Phys., 9, 8531–8543, doi:10.5194/acp-9-8531-2009, 2009.

Liu, J., Logan, J. A., Jones, D. B. A., Livesey, N. J., Megretskaia, I., Carouge, C., and Nedelec, P.: Analysis of CO in the tropical troposphere using Aura satellite data and the GEOS-Chem model: insights into transport characteristics of the GEOS meteorological products, Atmos. Chem. Phys., 10, 12207–12232, doi:10.5194/acp-10-12207-2010, 2010.

Liu, J., Logan, J. A., Murray, L. T., Pumphrey, H. C., Schwartz, M. J., and Megretskaia, I. A.: Transport analysis and source attribution of seasonal and interannual variability of CO in the tropical upper troposphere and lower stratosphere, Atmos. Chem. Phys., 13, 129–146, doi:10.5194/acp-13-129-2013, 2013.

Lupu, A., Kaminski, J. W., Neary, L., McConnell, J. C., Toyota, K., Rinsland, C. P., Bernath, P. F., Walker, K. A., Boone, C. D., Nagahama, Y., and Suzuki, K.: Hydrogen cyanide in the upper troposphere: GEM-AQ simulation and comparison with ACE-FTS observations, Atmos. Chem. Phys., 9, 4301–4313, doi:10.5194/acp-9-4301-2009, 2009.

Mahieu, E., Rinsland, C. P., Zander, R., Demoulin, P., Delbouille, L., and Roland, G.: Vertical column abundances of HCN

deduced from ground-based infrared solar spectra: long-term trend and variability, J. Atmos. Chem., 20, 299–310, 1995.

Mahieu, E., Zander, R., Delbouille, L., Demoulin, P., Roland, G., and Servais, C.: Observed trends in total vertical column abundances of atmospheric gases from IR solar spectra recorded at the Jungfraujoch, J. Atmos. Chem., 28, 227–243, 1997.

Morgenstern, O., Zeng, G., Wood, S. W., Robinson, J., Smale, D., Paton-Walsh, C., Jones, N. B., and Griffith, D. W. T.: Long-range correlations in Fourier transform infrared, satellite, and modeled CO in the Southern Hemisphere, J. Geophys. Res., 117, D11301, doi:10.1029/2012JD017639, 2012.

Mote, P. W., Rosenlof, K. H., McIntyre, M. E., Carr, E. S., Gille, J. C., Holton, J. R., Kinnersley, J. S., Pumphrey, H. C., Russell, J. M., and Waters, J. W.: An atmospheric tape recorder: the imprint of tropical tropopause temperatures on stratospheric water vapor, J. Geophys. Res., 101, 3989–4006, 1996.

Nett, H., Perron, G., Sanchez, M., Burgess, A., and Mossner, P.: MIPAS inflight calibration and processor validation, in ENVISAT Calibration Review – Proc. of the European Workshop, 9–13 September 2002, ESTEC, Noordwijk, the Netherlands, CD-ROM, vol. SP-520, edited by: Sawaya-Lacoste, H., ESA Publications Division, ESTEC, Noordwijk, the Netherlands, 2002.

Park, M., Randel, W. J., Emmons, L. K., Bernath, P. F., Walker, K. A., and Boone, C. D.: Chemical isolation in the Asian monsoon anticyclone observed in Atmospheric Chemistry Experiment (ACE-FTS) data, Atmos. Chem. Phys., 8, 757–764, doi:10.5194/acp-8-757-2008, 2008.

Park, M., Randel, W. J., Kinnison, D. E., Emmons, L. K., Bernath, P. F., Walker, K. A., Boone, C. D., and Livesey, N. J.: Hydrocarbons in the upper troposphere and lower stratosphere observed from ACE-FTS and comparisons with WACCM, J. Geophys. Res., 118, 1964–1980, doi:10.1029/2012JD018327, 2013.

Pommrich, R., Müller, R., Grooß, J. U., Günther, G., Konopka, P., Riese, M., Heil, A., Schultz, M., Pumphrey, H. C., and Walker, K. A.: What causes the irregular cycle of the atmospheric tape recorder signal in HCN?, Geophys. Res. Lett, 37, L16805, doi:10.1029/2010GL044056, 2010.

Pumphrey, H. C., Jimenez, C. J., and Waters, J. W.: Measurement of HCN in the middle atmosphere by EOS MLS, Geophys. Res. Lett., 33, L08804, doi:10.1029/2005GL025656, 2006.

Pumphrey, H. C., Boone, C., Walker, K. A., Bernath, P., and Livesey, N. J.: Tropical tape recorder observed in HCN, Geophys. Res. Lett, 35, L05801, doi:10.1029/2007GL032137, 2008.

Randel, W. J. and Jensen, E. J.: Physical processes in the tropical tropopause layer and their roles in a changing climate, Nature Geosci., 6, 169–176, doi:10.1038/ngeo1733, 2013.

Randel, W. J., Park, M., Emmons, L., Kinnison, D., Bernath, P., Walker, K. A., Boone, C., and Pumphrey, H.: Asian Monsoon transport of pollution to the stratosphere, Science, 328, 611–613, doi:10.1126/science.1182274, 2010.

Remedios, J. J., Leigh, R. J., Waterfall, A. M., Moore, D. P., Sembhi, H., Parkes, I., Greenhough, J., Chipperfield, M.P., and Hauglustaine, D.: MIPAS reference atmospheres and comparisons to V4.61/V4.62 MIPAS level 2 geophysical data sets, Atmos. Chem. Phys. Discuss., 7, 9973–10017, doi:10.5194/acpd-7-9973-2007, 2007.

Rinsland, C. P., Smith, M. A. H., Rinsland, P. L., Goldman, A., Brault, J. W., and Stokes, G. M.: Ground-based spectroscopic measurements of atmospheric hydrogen cyanide, J. Geophys. Res., 87, 11119–11125, 1982.

Rinsland, C. P., Gunson, M. R., Wang, P.-H., Arduini, R. F., Baum, B. A., Minnis, P., Goldman, A., Abrams, M. C., Zander, R., Mahieu, E., Salawitch, R. J., Michelsen, H. A., Irion, F. W., and Newchurch, M. J.: ATMOS/ATLAS 3 infrared measurements of trace gases in the November 1994 tropical and subtropical upper troposphere, J. Quant. Spectrosc. Ra., 60, 891–901, 1998.

Rinsland, C. P., Goldman, A., Murcray, F. J., Stephen, T. M., Pougatchev, N. S., Fishman, J., David S. J., Blatherwick, R. D., Novelli, P. C., Jones, N. B., and Connor, B. J.: Infrared solar spectroscopic measurements of free tropospheric CO, C_2H_6, and HCN above Mauna Loa, Hawaii: seasonal variations and evidence for enhanced emissions from the southeast Asian tropical fires of 1997–1998, J. Geophys. Res., 104, 18667–18680, 1999.

Rinsland, C. P., Mahieu, E., Zander, R., Demoulin, P., Forrer, J., and Buchmann, B.: Free tropospheric CO, C_2H_6, and HCN above central Europe: recent measurements from the Jungfraujoch station including the detection of elevated columns during 1998, J. Geophys. Res., 105, 24235–24249, 2000.

Rinsland, C. P., Goldman, A., Zander, R., and Mahieu, E.: Enhanced tropospheric HCN columns above Kitt Peak during the 1982–1983 and 1997–1998 El Niño warm phases, J. Quant. Spectrosc. Ra., 69, 3–8, 2001a.

Rinsland, C. P., Meier, A., Griffith, D. W. T., and Chiou, L. S.: Ground-based measurements of tropospheric CO, C_2H_6, and HCN from Australia at 34° S latitude during 1997–1998, J. Geophys. Res., 106, 20913–20924, 2001b.

Rinsland, C. P., Jones, N. B., Connor, B. J., Wood, S. W., Goldman, A., Stephen, T. M., Murcray, F. J., Chiou, L. S., Zander, R., and Mahieu, E.: Multiyear infrared solar spectroscopic measurements of HCN, CO, C_2H_6, and C_2H_2 tropospheric columns above Lauder, New Zealand (45° S latitude), J. Geophys. Res., 107, 4185, doi:10.1029/2001JD001150, 2002.

Rinsland, C. P., Dufour, G., Boone, C. D., and Bernath, P. F.: Atmospheric Chemistry Experiment (ACE) measurements of elevated Southern Hemisphere upper tropospheric CO, C_2H_6, HCN, and C_2H_2 mixing ratios from biomass burning emissions and long range transport, Geophys. Res. Lett., 32, L20803, doi:10.1029/2005GL024214, 2005.

Rothman, L. S., Gordon, I. E., Babikov, Y., et al.: The HITRAN2012 molecular spectroscopic database, J. Quant. Spectrosc. Ra., 130, 4–50, doi:10.1016/j.jqsrt.2013.07.002, 2013.

Schoeberl, M. R., Duncan, B. N., Douglass, A. R., Waters, J., Livesey, N., Read, W., and Filipiak, M.: The carbon monoxide tape recorder, Geophys. Res. Lett., 33, L12811, doi:10.1029/2006GL026178, 2006.

Schoeberl, M. R., Douglass, A. R., Stolarski, R. S., Pawson, S., Strahan, S. E., and Read, W.: Comparison of lower stratospheric tropical mean vertical velocities, J. Geophys. Res., 113, D24109, doi:10.1029/2008JD010221, 2008.

Singh, H. B., Herlth, D., Kolyer, R., Chatfield, R., Viezee, W., Salas, L. J., Chen, Y., Bradshaw, J. D., Sandholm, S. T., Talbot, R., Gregory, G. L., Anderson, B., Sachse, G. W., Browell, E., Bachmeier, A. S., Blake, D. R., Heikes, B., Jacob, D., and H. E. Fuelberg: Impact of biomass burning emissions on the composition of the South Atlantic troposphere: reactive nitrogen and ozone, J. Geophys. Res., 101, 24203–24219, 1996.

Singh, H. B., Viezee, W., Chen, Y., Bradshaw, J., Sandholm, S., Blake, D., Blake, N., Heikes, B., Snow, J., Talbot, R., Browell, E., Gregory, G., Sachse, G., and Vay, S.: Biomass burning influences on the composition of the remote South Pacific troposphere: analysis based on observations from PEM-Tropics-A, Atmos. Environ., 34, 635–644, 2000.

Singh, H. B., Salas, L., Herlth, D., Kolyer, R., Czech, E., Viezee, W., Li, Q., Jacob, D. J., Blake, D., Sachse, G., Harward, C. N., Fuelberg, H., Kiley, C. M., Zhao, Y., and Kondo, Y.: In situ measurements of HCN and CH_3CN over the Pacific Ocean: sources, sinks and budgets, J. Geophys. Res., 108, 8795, doi:10.1029/2002JD003006, 2003.

Singh, H. B., Brune, W. H., Crawford, J. H., Flocke, F., and Jacob, D. J.: Chemistry and transport of pollution over the Gulf of Mexico and the Pacific: spring 2006 INTEX-B campaign overview and first results, Atmos. Chem. Phys., 9, 2301–2318, doi:10.5194/acp-9-2301-2009, 2009.

Steck, T.: Methods for determining regularization for atmospheric retrieval problems, Appl. Optics, 41, 1788–1797, 2002.

Stiller, G. P. (Ed.): The Karlsruhe Optimized and Precise Radiative transfer Algorithm (KOPRA), Wissenschaftliche Berichte, vol. FZKA 6487, Forschungszentrum Karlsruhe GmbH, 2000.

Stohl, A., Berg, T., Burkhart, J. F., Fjǽraa, A. M., Forster, C., Herber, A., Hov, Ø., Lunder, C., McMillan, W. W., Oltmans, S., Shiobara, M., Simpson, D., Solberg, S., Stebel, K., Ström, J., Tørseth, K., Treffeisen, R., Virkkunen, K., and Yttri, K. E.: Arctic smoke – record high air pollution levels in the European Arctic due to agricultural fires in Eastern Europe in spring 2006, Atmos. Chem. Phys., 7, 511–534, doi:10.5194/acp-7-511-2007, 2007.

Tereszchuk, K. A., González Abad, G., Clerbaux, C., Hadji-Lazaro, J., Hurtmans, D., Coheur, P.-F., and Bernath, P. F.: ACE-FTS observations of pyrogenic trace species in boreal biomass plumes during BORTAS, Atmos. Chem. Phys., 13, 4529–4541, doi:10.5194/acp-13-4529-2013, 2013.

von Clarmann, T., Fischer, H., Funke, B., Glatthor, N., Grabowski, U., Höpfner, M., Kellmann, S., Kiefer, M., Linden, A., Mengistu Tsidu, G., Milz, M., Steck, T., Stiller, G. P., Wang, D.-Y., Gil-López, S., and López-Puertas, M.: Retrieval of temperature and tangent altitude pointing from limb emission spectra recorded from space by the Michelson Interferometer for Passive Atmospheric Sounding (MIPAS), J. Geophys. Res., 108, doi:10.1029/2003JD003602, 2003.

von Clarmann, T., Glatthor, N., Koukouli, M. E., Stiller, G. P., Funke, B., Grabowski, U., Höpfner, M., Kellmann, S., Linden, A., Milz, M., Steck, T., and Fischer, H.: MIPAS measurements of upper tropospheric C_2H_6 and O_3 during the southern hemispheric biomass burning season in 2003, Atmos. Chem. Phys., 7, 5861–5872, doi:10.5194/acp-7-5861-2007, 2007.

van der Werf, G. R., Randerson, J. T., Giglio, L., Collatz, G. J., Kasibhatla, P. S., and Arellano Jr., A. F.: Interannual variability in global biomass burning emissions from 1997 to 2004, Atmos. Chem. Phys., 6, 3423–3441, doi:10.5194/acp-6-3423-2006, 2006.

van der Werf, G. R., Randerson, J. T., Giglio, L., Collatz, G. J., Mu, M., Kasibhatla, P. S., Morton, D. C., DeFries, R. S., Jin, Y., and van Leeuwen, T. T.: Global fire emissions and the contribution of deforestation, savanna, forest, agricultural, and peat fires (1997–2009), Atmos. Chem. Phys., 10, 11707–11735, doi:10.5194/acp-10-11707-2010, 2010.

Warneke, C., Froyd, K. D., Brioude, J., Bahreini, R., Brock, C. A., Cozic, J., de Gouw, J. A., Fahey, D. W., Ferrare, R., Holloway, J. S., Middlebrook, A. M., Miller, L., Montzka, S., Schwarz, J .P., Sodemann, H., Spackman, J. R., and Stohl, A.: An important contribution to springtime Arctic aerosol from biomass burning in Russia, Geophys. Res. Lett., 37, L01801, doi:10.1029/2009GL041816, 2010.

Wiegele, A., Glatthor, N., Höpfner, M., Grabowski, U., Kellmann, S., Linden, A., Stiller, G., and von Clarmann, T.: Global distributions of C_2H_6, C_2H_2, HCN, and PAN retrieved from MIPAS reduced spectral resolution measurements, Atmos. Meas. Tech., 5, 723–734, doi:10.5194/amt-5-723-2012, 2012.

Worden, H. M., Deeter, M. N., Frankenberg, C., George, M., Nichitiu, F., Worden, J., Aben, I., Bowman, K. W., Clerbaux, C., Coheur, P. F., de Laat, A. T. J., Detweiler, R., Drummond, J. R., Edwards, D. P., Gille, J. C., Hurtmans, D., Luo, M., Martínez-Alonso, S., Massie, S., Pfister, G., and Warner, J. X.: Decadal record of satellite carbon monoxide observations, Atmos. Chem. Phys., 13, 837–850, doi:10.5194/acp-13-837-2013, 2013.

Yokelson, R. J., Urbanski, S. P., Atlas, E. L., Toohey, D. W., Alvarado, E. C., Crounse, J. D., Wennberg, P. O., Fisher, M. E., Wold, C. E., Campos, T. L., Adachi, K., Buseck, P. R., and Hao, W. M.: Emissions from forest fires near Mexico City, Atmos. Chem. Phys., 7, 5569–5584, doi:10.5194/acp-7-5569-2007, 2007.

Zeng, G., Wood, S. W., Morgenstern, O., Jones, N. B., Robinson, J., and Smale, D.: Trends and variations in CO, C_2H_6, and HCN in the Southern Hemisphere point to the declining anthropogenic emissions of CO and C_2H_6, Atmos. Chem. Phys., 12, 7543–7555, doi:10.5194/acp-12-7543-2012, 2012.